Sequence action representations contextualize during rapid skill learning.

Debadatta Dash[1], Fumiaki Iwane[1], William Hayward[1], Roberto Salamanca-Giron[1], Marlene Bonstrup[2], Ethan Buch[1]*, and Leonardo G Cohen[1]*

[1]Human Cortical Physiology and Neurorehabilitation Section, NINDS, NIH, USA

[2]Department of Neurology, University of Leipzig Medical Center, Leipzig, Germany

*To whom correspondence should be addressed

cohenl@ninds.nih.gov, ethan.buch@nih.gov

Declaration of interests. The authors declare no competing interests.

Abstract

Activities of daily living rely on our ability to acquire new motor skills composed of precise action sequences. Early learning of a new sequential skill is characterized by steep performance improvements that develop predominantly during rest intervals interspersed with practice, a form of rapid consolidation. Here, we ask if the millisecond level neural representation of an action performed at different locations within a skill sequence contextually differentiates or remains stable as learning evolves. Optimization of machine learning decoders to classify sequence-embedded finger movements from MEG activity reached approximately 94% accuracy. The representation manifolds of the same action performed in different sequence contexts progressively differentiated during rest periods of early learning, predicting skill gains. We conclude that sequence action representations contextually differentiate during early skill learning, an issue relevant to brain-computer interface applications in neurorehabilitation.

Introduction

Motor learning is required to perform a wide array of basic daily living activities, intricate athletic endeavors, and professional skills. Whether it's learning to type more quickly on a keyboard[1], improve one's tennis game[2], or play a piece of music on the piano[3] – all of these skills require the ability to execute sequences of actions with precise temporal coordination. Action sequences thus form the building blocks of fine motor skills[4]. Initial exposure to acquisition of a new skill results in rapid performance improvements during the initial practice session (i.e. – early learning), which is up to four times larger in magnitude compared to offline performance improvements reported following overnight sleep[1,5].

Recent work advanced our understanding of the mechanisms supporting early skill learning. The density of fast hippocampo-neocortical skill memory replay events increases approximately three-fold during rest periods of early learning with their density explaining differences in the magnitude of micro-offline gains across subjects[6]. Jacobacci et al. (2020)[7] reported BOLD fMRI changes in the hippocampus and precuneus (regions also identified using MEG)[6] linked to micro-offline gains. These functional changes were coupled with rapid alterations in brain microstructure in the order of minutes, suggesting that the same network that operates during rest periods of early learning undergoes structural plasticity over several minutes following practice[8]. Chen et al. (2024)[9] and Sjøgård et al (2024)[10] provided crucial direct evidence from intracranial EEG in humans linking sharp-wave ripple density during rest periods (known markers for neural replay)[11] in the human hippocampus (80-120 Hz) to micro-offline gains during early learning. Thus, converging evidence now links hippocampal activity, neural replay dynamics, and micro-offline performance gains as mechanisms supporting rapid consolidation during early learning.

The neural representation of a sequential skill binds discrete individual actions (e.g. - single piano keypress) into complex, temporally and spatially precise sequence representations (e.g. - a refrain from a piece of music)[12,13]. The neural representation or manifold[14] of sequential skills has been characterized in humans[3,15,16]. Previous fMRI reports showed that the representation of individual motor sequence actions may remain relatively stable over days or weeks of practice, after a memory is formed[17]. However, it is not known if individual sequence action representations differentiate or remain stable during early skill learning, when most prominent performance improvements occur, and the memory is not yet fully formed[1]. Furthermore, it is not known if the neural representations for identical movements occurring at different positions of a sequential skill

differentiate (or contextualize) as a function of learning, an issue crucial to the robustness of BCI applications.

Investigating the contextualization of discrete action representations at a millisecond level is challenging since both the individual actions and the skill sequence they are embedded within are concurrently represented in changing neural activity dynamics during learning[16,18]. To address this problem, we constructed a series of decoders aimed at predicting keypress actions from magnetoencephalographic (MEG) neural activity, dependent upon the learning state and the local sequence context (ordinal position) the keypress action is performed within. Implementing this novel approach allowed us to determine that individual sequence actions are indeed contextualized during early skill learning resulting in differentiation of their neural representations, and that the degree of this differentiation predicts skill gains. This representational contextualization was also observed to predominantly develop during rest rather than during practice intervals in parallel with rapid consolidation of skill.

Results

Participants engaged in a well characterized sequential skill learning task[1,5,6] that involved repetitive typing of a sequence (4-1-3-2-4) performed with their (non-dominant) left hand over 36 trials with alternating periods of 10s *practice* and 10s *rest* (*inter-practice rest*; *Day 1 Training*; **Figure 1A**). Individual keypress times and finger keypress identities were recorded and used to quantify skill as the correct sequence speed (keypresses/s)[1].

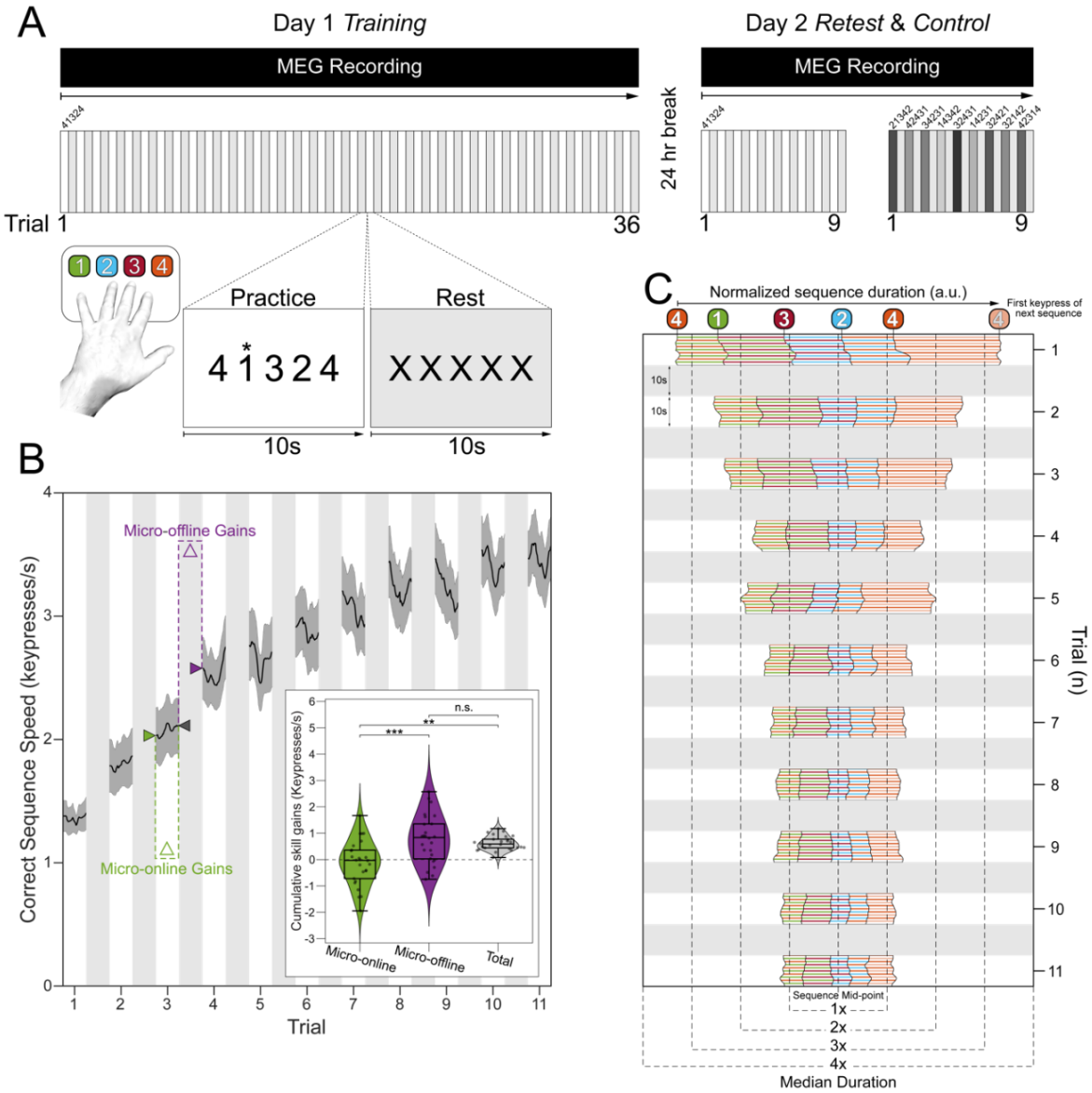

Figure 1. Experimental design and behavioral performance. *A. Skill learning task.* Participants engaged in a procedural motor skill learning task, which required them to repeatedly type a keypress sequence, "4 − 1 − 3 − 2 − 4" (1 = little finger, 2 = ring finger, 3 = middle finger, and 4 = index finger) with their non-dominant, left hand. The *Day 1 Training* session included 36 trials, with each trial consisting of alternating 10s practice and rest intervals. After a 24-hour break, participants were retested on performance of the same sequence (4-1-3-2-4) for 9 trials (*Day 2 Retest)* as well as single-trial performance on 9 different sequences (*Day 2 Control*; 2-1-3-4-2, 4-2-4-3-1, 3-4-2-3-1, 1-4-3-4-2, 3-2-4-3-1, 1-4-2-3-1, 3-2-4-2-1, 3-2-1-4-2, and 4-2-3-1-4). MEG was recorded during both Day 1 and Day 2 sessions with a 275-channel CTF magnetoencephalography (MEG) system (CTF Systems, Inc., Canada). ***B. Skill***

Learning. As reported previously[1], participants on average reached 95% of peak performance by trial 11 of the *Day 1 Training* session (see **Figure 1 - figure supplement 1A** for results over all *Day 1 Training* and *Day 2 Retest* trials). At the group level, total early learning was exclusively accounted for by micro-offline gains during inter-practice rest intervals (Figure 1B inset). **C. Keypress transition time (KTT) variability.** Distribution of KTTs normalized to the median correct sequence time for each participant and centered on the mid-point for each full sequence iteration during early learning (see **Figure 1—figure supplement 1B** for results over all *Day 1 Training* and *Day 2 Retest* trials). Note the initial variability of the relative KTT composition of the sequence (i.e. – 4-1, 1-3, 3-2, 2-4, 4-4), before it stabilizes by trial 6 in the early learning period.

Participants reached 95% of maximal skill (i.e. - Early Learning) within the initial 11 practice trials (**Figure 1B)**, with improvements developing over inter-practice rest periods (micro-offline gains) accounting for almost all of total learning across participants (**Figure 1B inset**)[1]. In addition to the reduction in sequence duration during early learning, the relative duration of component keypress transitions displayed increased temporal regularity across sequence iterations (**Figure 1C**). On average across subjects, 2.32% ± 1.48% (mean ± SD) of all keypresses performed were errors, which were evenly distributed across the four possible keypress responses. While errors increased progressively over practice trials, they did so in proportion to the increase in correct keypresses, so that the overall ratio of correct-to-incorrect keypresses remained stable over the training session.

On the following day, participants were retested on performance of the same sequence (4-1-3-2-4) over 9 trials (*Day 2 Retest*), as well as single-trial performance on 9 different untrained sequences (*Day 2 Controls*: 2-1-3-4-2, 4-2-4-3-1, 3-4-2-3-1, 1-4-3-4-2, 3-2-4-3-1, 1-4-2-3-1, 3-2-4-2-1, 3-2-1-4-2, and 4-2-3-1-4). As expected, an upward shift in performance of the trained sequence (0.68 ± SD 0.56 keypresses/s; $t = 7.21$, $p < 0.001$) was observed during *Day 2 Retest*, indicative of an overnight skill consolidation effect for the trained sequence (**Figure 1 - figure supplement 1A**).

Keypress actions are represented in multi-scale hybrid-space manifolds.

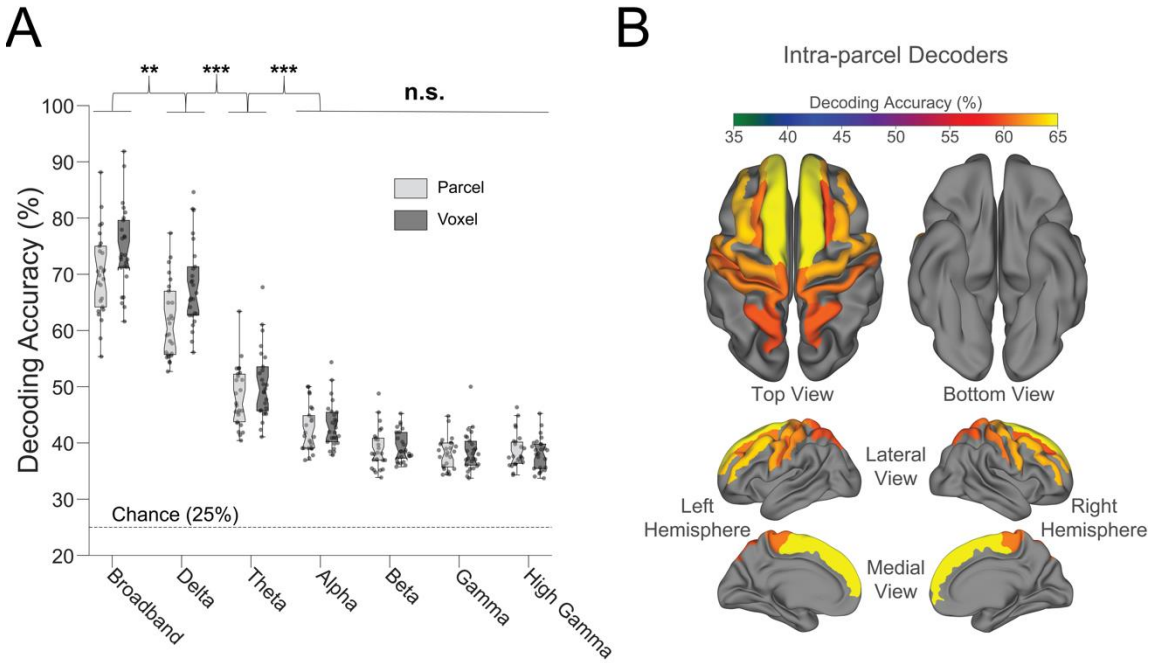

Figure 2. Spatial and oscillatory contributions to neural decoding of finger identities *A. Contribution of whole brain oscillatory frequencies to decoding.* When trained on broadband activity relative to narrow frequency band features, decoding accuracy (i.e. - test sample performance) was highest for whole-brain voxel- (74.51% ± SD 7.34%, t = 8.08, $p < 0.001$) and parcel-space (70.11% ± SD 7.11%, t = 13.22, $p < 0.001$) MEG activity. Thus, decoders trained on whole-brain broadband data consistently outperformed those trained on narrowband activity. Dots depict decoding accuracy for each participant. *$p < 0.05$, **$p < 0.01$, ***$p < 0.001$, ns.: not significant. ***B. Contribution of intra-parcel brain oscillatory frequencies to decoding.*** Performance of the top performing decile of intra-parcel decoders (see **Methods**, **Figure 2—figure supplement 1**) over different frequency bands (top-panel; decoding accuracy is color coded and listed for each parcel and frequency band assessed). Broadband activity resulted in best accuracy closely followed by delta band activity. Broadband intra-parcel decoding accuracy mapped to a standard brain surface (FreeSurfer *fsaverage* brain) and color-coded by accuracy (bottom panel). Note that bilateral superior frontal cortex (yellow, 69%) contributed the most to decoding accuracy followed by middle frontal, pre-and post-central regions (> 60%).

To investigate the possibility of contextualization of neural representations, we constructed a set of decoders to predict keypress actions from MEG activity as a function of both the learning state and the ordinal position of the keypress within the sequence. We first characterized the spectral and spatial features of keypress state representations by comparing performance of decoders constructed around broadband (1-100Hz) or narrowband [delta- (1-3Hz), theta- (4-7Hz), alpha- (8-14 Hz), beta- (15-24 Hz), gamma- (25-50Hz) and high gamma-band (51-100Hz)] MEG oscillatory activity. We found that decoders trained on broadband data consistently outperformed those trained on narrowband activity, and that whole-brain parcel- (148 brain regions or parcels) or voxel-space (15684 voxels)[19] decoders exhibited greater accuracy (parcel: t = 1.89, $p = 0.035$, df = 25, Cohen's d = 0.17; voxel: t = 7.18, $p < 0.001$, df = 25, Cohen's d = 0.76) than individual voxel-space intra-parcel decoders (**Figure 2**). Specifically, while the highest performing intra-parcel decoders predicted keypresses with up to 68.77% (± SD 7.6%) accuracy, whole-brain inter-parcel decoder accuracy reached 74.51% (± SD 7.34%) (**Figure 2,** also see **Figure 2 – figure supplement 1)**.

Next, we asked if the combination of intra- and inter-parcel activity patterns, constituting a multi-scale hybrid space**,** improve further keypress predictions. We constructed hybrid space decoders (N = 1295 ± 20) combining all inter-parcel activity with top-ranked intra-parcel features (covering 8 regions, see **Methods**, **Figure 3A**). Decoder accuracy was higher for hybrid (78.15% ± SD 7.03% accuracy and a weighted mean F1 score of 0.78 ± SD 0.07) than for voxel- (74.51% ± SD 7.34%; paired *t*-test: t = 6.30, $p < 0.001$, df = 25, Cohen's d = 0.39) and parcel- (70.11% ± SD 7.48%; paired *t*-test = 12.08, $p < 0.001$, df = 25, Cohen's d = 0.98) spaces (**Figure 3B, Figure 3 – figure supplement 1**). Thus, a multi-scale hybrid-space representation best characterizes keypress action manifolds.

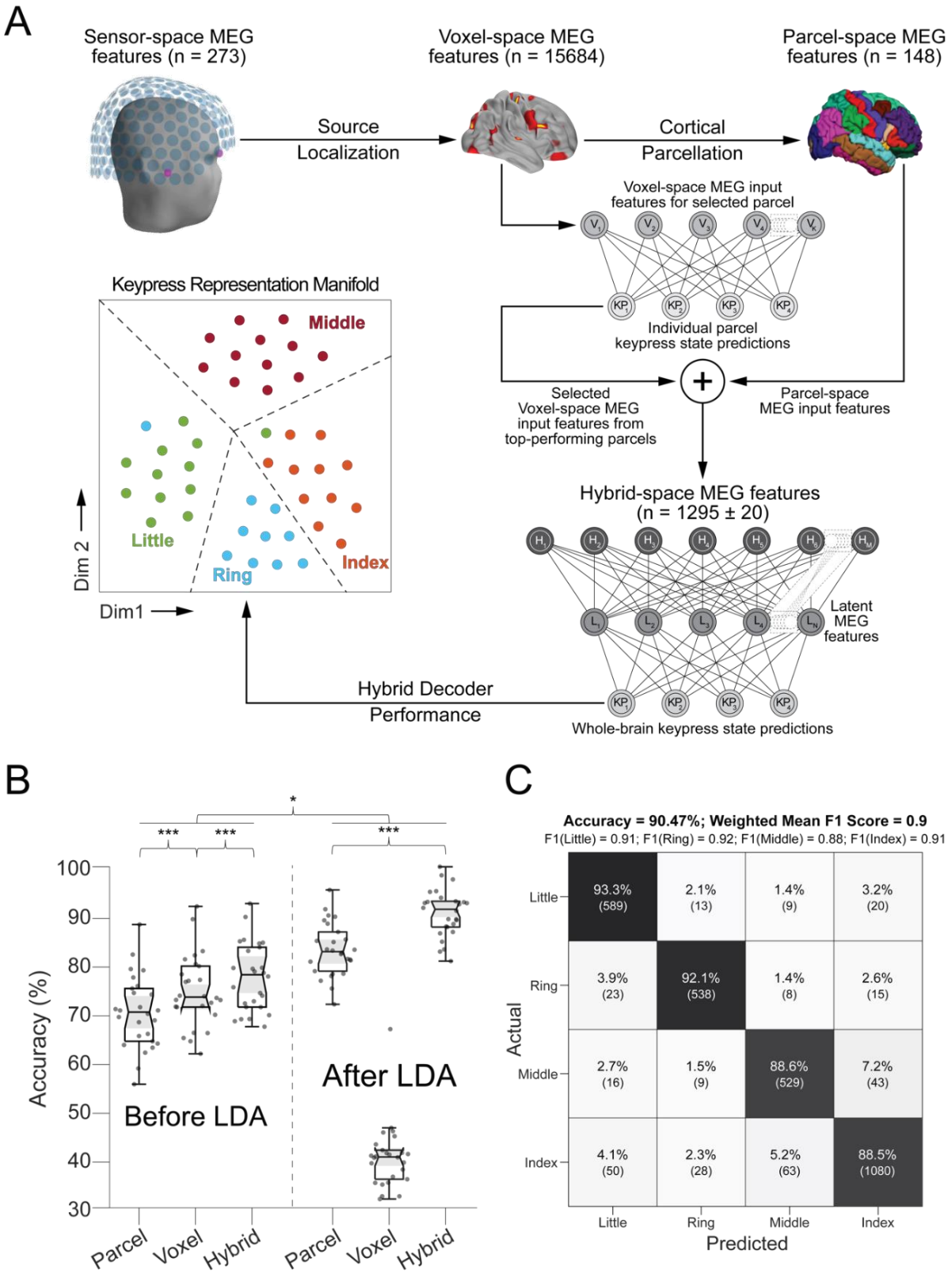
A
Sensor-space MEG features (n = 273)
Source Localization
Voxel-space MEG features (n = 15684)
Cortical Parcellation
Parcel-space MEG features (n = 148)
Voxel-space MEG input features for selected parcel
Individual parcel keypress state predictions
Selected Voxel-space MEG input features from top-performing parcels
Parcel-space MEG input features
Hybrid-space MEG features (n = 1295 ± 20)
Latent MEG features
Whole-brain keypress state predictions
Hybrid Decoder Performance
Keypress Representation Manifold
Middle
Little
Ring
Index
Dim 1
Dim 2
B
Accuracy (%)
Before LDA
After LDA
Parcel
Voxel
Hybrid
C
Accuracy = 90.47%; Weighted Mean F1 Score = 0.9
F1(Little) = 0.91; F1(Ring) = 0.92; F1(Middle) = 0.88; F1(Index) = 0.91
Actual
Predicted
Little
Ring
Middle
Index
93.3% (589)
2.1% (13)
1.4% (9)
3.2% (20)
3.9% (23)
92.1% (538)
1.4% (8)
2.6% (15)
2.7% (16)
1.5% (9)
88.6% (529)
7.2% (43)
4.1% (50)
2.3% (28)
5.2% (63)
88.5% (1080)

Figure 3. Hybrid spatial approach for neural decoding during skill learning *A. Pipeline*. Sensor-space MEG data (N = 272 channels) were source-localized (voxel-space features; N = 15684 voxels), and then parcellated (parcel-space features; N = 148) by averaging the activity of all voxels located within an individual region defined in a standard template space (Desikan-Killiany Atlas). Individual voxel-space regional decoders (intra-parcel decoders) were then constructed and ranked. The final hybrid-space keypress state (i.e. – 4-class) decoder was constructed using all parcel-spaces and top-ranked intra-parcel voxel input features (see Methods). **B. Decoding performance across parcel, voxel, and hybrid spaces.** Note that decoding performance was highest for the hybrid space approach compared to performance obtained for whole-brain voxel- and parcel spaces. Addition of linear discriminant analysis (LDA)-based dimensionality reduction further improved decoding performance for both parcel- and hybrid-space approaches. Each dot represents accuracy for a single participant and method. "∗∗∗" indicates $p < 0.001$ and "∗" indicates $p < 0.05$. ***C. Confusion matrix of individual finger identity decoding for hybrid-space manifold features.*** True predictions are located on the main diagonal. Off-diagonal elements in each row depict false-negative predictions for each finger, while off-diagonal elements in each column indicate false-positive predictions. Please note that the index finger keypress had the highest misclassifications (n = 141 or 47.5% of all prediction errors).

We implemented several dimensionality reduction or manifold extraction strategies including principal component analysis (PCA), multi-dimensional scaling (MDS), minimum redundant maximum relevance (MRMR), and linear discriminant analysis (LDA)[20] to map the input feature (parcel, voxel, or hybrid) space to a low-dimensional latent space[14]. LDA-based manifold extraction led to the greatest classifier performance gains, improving keypress decoding accuracy to 90.47% ± SD 4.84% (**Figure 3B**; weighted mean F1 score = 0.91 ± SD 0.05). In comparison, LDA-based dimensionality reduction also improved parcel-space decoder performance (82.95% ± SD 5.48%) but reduced voxel-space decoder accuracy (40.38 % ± SD 6.78%; also see **Figure 3 – figure supplement 2**). Notably, decoding of index finger keypresses (executed at two different ordinal positions in the sequence) exhibited the highest false negative (0.116 per keypress) and false positive (0.043 per keypress) misclassification rates compared with all other digits (false

negative rate range = [0.067 0.114]; false positive rate range = [0.020 0.037]; **Figure 3C**), raising the hypothesis that the same action could be differentially represented when executed within different contexts (i.e. - different learning states or sequence locations).

We assessed the robustness of this hybrid strategy for decoding individual actions during skill learning over multiple sessions by applying it to data collected on the following day during the *Day 2 Retest* (9-trial retest of the same trained sequence) and *Day 2 Control* (single-trial performance of 9 different untrained sequences) blocks. The decoding accuracy for *Day 2* MEG data remained high (87.11% ± SD 8.54% for the trained sequence during *Retest*, and 79.44% ± SD 5.54% for the untrained *Control* sequences; see confusion matrices in **Figure 3 – figure supplement 3**). This indicates that the hybrid decoding strategy is particularly reliable for decoding keypress actions during skill learning and the neural representations of the learned sequence remain stable the following day. Although the keypress state decoding performance was lower for untrained *Control* sequences relative to the trained sequence, greater accuracy of the hybrid approach over purely parcel- or voxel-space input features was still observed. Thus, this hybrid approach allows robust sequential finger movement decoding across multiple days and sequences.

Inclusion of keypress sequence context location optimized decoding performance.

Next, we tracked the trial-by-trial evolution of keypress action manifolds as training progressed. Keypress neural representations were observed to progressively differentiate during early learning (**Figure 4**). A representative example in **Figure 4A** (top row) depicts progressive representational clustering of four-digit representations from trials 1, 11, and 36. The spatial representation of these clusters changed over the course of training, from predominant involvement of pre-central areas in trial 1 to post-central, superior, and middle frontal cortex contributions in later trials 11 and 36

(**Figure 4A**, bottom row). Thus, a shift in activity from pre-central areas to post-central, superior, and middle frontal cortex paralleled improvements in decoding performance (also see **Figure 4 – figure supplement 1** for trial-by-trial quantitative feature importance score changes during skill learning).

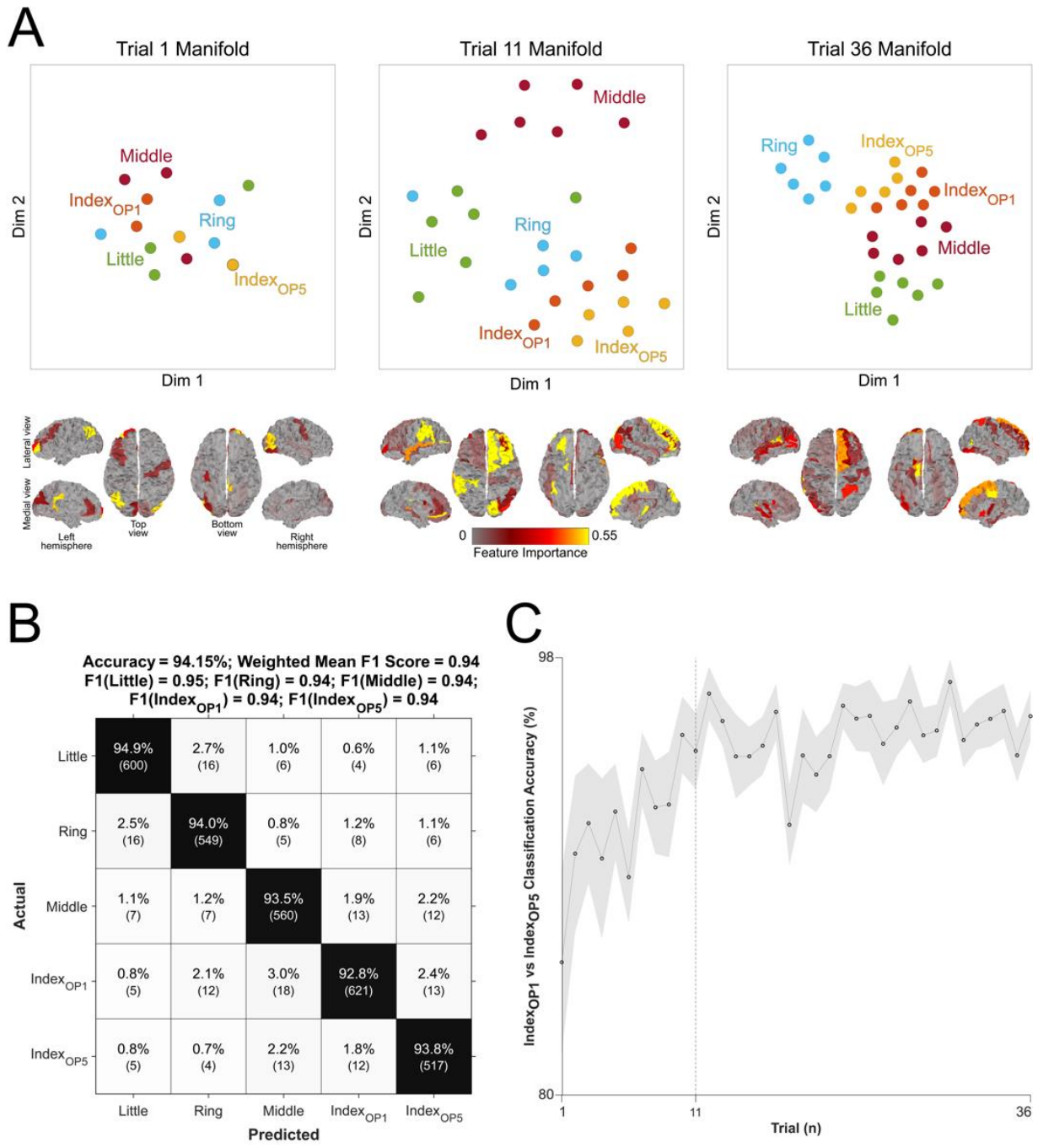

Figure 4. Evolution of keypress neural representations with skill learning ***A. Keypress neural representations differentiate during early learning.*** t-SNE distribution of neural representation of each keypress (top scatter plots) is shown for trial 1 (start of training; top-left), 11 (end of early learning; top-center), and 36 (end of training; top-right) for a single representative participant. Individual keypress manifold representation clustering in trial 11 (top-center; end of early learning) depicts sub-clustering for the index finger keypress performed at the two different ordinal positions in the sequence ($Index_{OP1}$ and $Index_{OP5}$), which remains present by trial 36 (top-right). Spatial distribution of regional contributions to decoding (bottom brain surface maps). The surface color heatmap indicates feature importance scores across the brain. Note that decoding contributions shifted from right pre-central cortex at trial 1 (bottom-left) to superior and middle frontal cortex at trials 11 (bottom-center) and 36 (bottom-right). ***B. Confusion matrix for 5-class decoding of individual sequence items.*** Decoders were trained to classify contextual representations of the keypresses (i.e., 5-class classification of the sequence elements 4-1-2-3-4). Note that the decoding accuracy increased to 94.15% ± SD 4.84% and the misclassification of keypress 4 was significantly reduced (from 141 to 82). ***C. Trial-by-trial classification accuracy for 2-class decoder ($Index_{OP1}$ vs. $Index_{OP5}$).*** A decoder trained to differentiate between the two index finger keypresses embedded at different positions ($Index_{OP1}$ at ordinal position 1 vs. $Index_{OP5}$ at ordinal position 5) within the trained sequence becomes progressively more accurately over early learning, stabilizing around 96% by trial 12 (end of early learning). Taken together, these findings indicate that the neural feature space evolves over early learning to incorporate sequence location information.

Correct performance of the training sequence required pressing the index finger twice (**4**-1-3-2-**4**) at two contextually different ordinal positions (sequence positions 1 and 5). Inclusion of sequence location information (i.e. – sequence context) for each keypress action (five sequence elements with the one keypress represented twice at two different locations) improved decoding accuracy (t = 7.09, $p < 0.001$, df = 25, Cohen's d = 0.86, **Figure 4B)** from 90.47% (± SD 3.44%) to 94.15% (± SD 4.84%; weighted mean F1 score: 0.94), and reduced overall misclassifications by 54.3% (from 219 to 119; **Figure 3C and 4B**). This is supported by greater differentiation in neural representations of the two different index finger keypresses embedded at different points within the sequence (**Figure 4A**), which leads to a trial-by-trial increase in 2-class decoding accuracy

(**Figure 4C**). Inclusion of contextual information to the hybrid-space decoder also increased classification accuracy of Day 2 Retest trained sequence data (from 87.11% for 4-class to 90.22% for 5-class). As expected, contextualized 5-class decoding of Day 2 Control MEG data for untrained sequences performed at or below chance levels (≤ 30.22% ± SD 0.44%) due to varied ordinal positions of keypress actions across the different sequences. Thus, inclusion of contextual information in the decoding framework only improves decoding accuracy for skill sequences which have been learned through practice.

Neural representation of keypress sequence location diverged during early skill learning. Finally, we used a Euclidian distance measure to evaluate the differentiation of the neural representation manifold of the same action (i.e. - an index-finger keypress) executed within different local sequence contexts (i.e. - ordinal position 1 vs. ordinal position 5). Note that, the neural representation manifolds (i.e. - the reduced dimension hybrid-space features extracted from broadband MEG data) are the features that resulted in the best decoding performance (See Methods, **Figure 3 – figure supplement 2**).

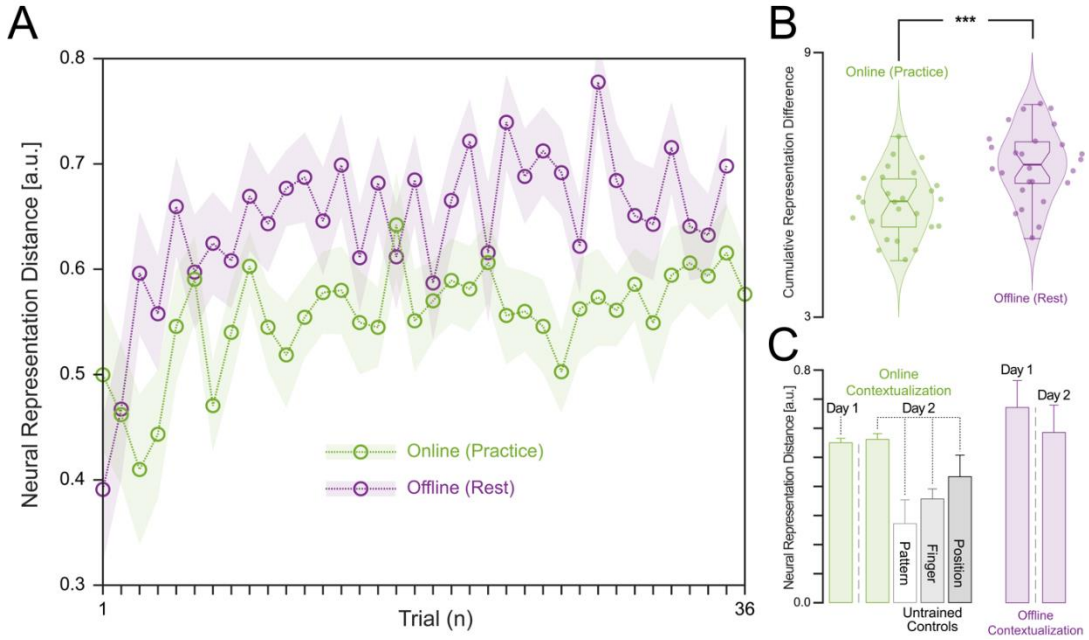

Figure 5: Neural representation distance between index finger keypresses performed at two different ordinal positions within a sequence. A. *Contextualization increases over Early Learning during Day 1 Training*. Online (Practice; green line) and offline (Rest; magenta line) neural representation distances between two index finger key presses performed at ordinal positions 1 and 5 of the trained sequence (4-1-3-2-4) are shown for each trial during Day 1 Training. Both online and offline distances between the two index finger representations increase sharply over the Early Learning before stabilizing across later *Day 1 Training* trials. **B. *Contextualization primarily occurs offline during short inter-practice rest periods.*** The neural representation difference was significantly greater when assessed offline (right distribution; purple) versus online (left distribution; green) periods (t = 4.84, $p < 0.001$, df = 25, Cohen's d= 1.2). **C. *Contextualization was retained after 24 hours and was specific to the trained sequence.*** The neural representation differences assessed across both rest and practice for the trained sequence (4-1-3-2-4) were retained for *Day 2 Retest*. Further, contextualization was significantly reduced for several untrained sequences controlling for: 1) index finger keypresses located at the same ordinal positions 1 and 5 but with a different intervening sequence pattern (*Pattern Specificity Control*: 4-2-3-1-4); 2) both ordinal 1 and 5 position keypresses performed with either the little or ring finger instead of the index finger (*Finger Specificity Control*: 2-1-3-4-2, 1-4-2-3-1 and 2-3-1-4-2); and 3) multiple index finger keypresses occurring at ordinal positions other than 1 and 5 (*Position Specificity Control*: 4-2-4-3-1 and 1-4-3-4-2). The mean online neural representation distance, or degree of contextualization, was substantially lower for the untrained control sequences (51.05% lower for the *Pattern Specificity Control* sequence, 35.80% lower for the *Finger Specificity Control* sequences, and 22.06% lower for the *Position Specificity Control* sequences) compared with the trained sequence. Note that offline contextualization cannot be measured for the *Day 2 Control* sequences as each sequence was only performed over a single trial.

The Euclidian distance between keypress sequence location manifolds of the index finger in its two ordinal positions increased progressively during both rest and practice periods of early learning before stabilizing (**Figure 5A**). Change in this Euclidian distance was more prominent during rest than during practice periods (t = 4.84, $p < 0.001$, df = 25, Cohen's d = 1.2; **Figure 5B**), similar to early learning gains (**Figure 1B**) and strongly predicted cumulative micro-offline gains ($r = 0.90$, $R^2 = 0.82$, $p < 0.001$; **Figure 5 - figure supplement 1**). Importantly, the differentiation in neural representations was not explained by differences in keypress transition pattern regularity

(within-subject; t = -0.03, p = 0.976; **Figure 5 – figure supplement 2**) or typing speed (between-subject; R^2 = 0.028, p = 0.41; **Figure 5 – figure supplement 3**). We further evaluated individual subject correlations between 1) contextualization changes during rest intervals and micro-offline gains; 2) contextualization changes during practice trials and micro-online gains, and 3) contextualization changes during practice trials and micro-offline gains (**Figure 5 – figure supplement 4**). Within-subject correlations between contextualization changes during rest intervals and micro-offline gains were significantly higher than between 1) online contextualization and micro-online gains (t = 3.2827, p = 0.0015, df = 25, Cohen's d = 1.2) and 2) online contextualization and micro-offline gains (t = 3.7021, p = 5.3013e-04, df = 25, Cohen's d = 0.69). Further, when quantifying online changes in contextualization from the first Index_{OP1} to the last Index_{OP5} keypress in the same trial we observed no learning-related trend (**Figure 5 – figure supplement 5, right panel**). Importantly, offline distances were significantly larger than online distances regardless of the measurement approach and neither predicted online learning (**Figure 5 – figure supplement 6**).

The neural representation differences assessed across both rest and practice for the trained sequence (4-1-3-2-4) were retained for *Day 2 Retest* **(Figure 5C)**. Comparatively, contextualization was reduced for several untrained sequences controlling for intervening sequence patterns (*Pattern Specificity Control*: 4-2-3-1-4), keypresses performed at the same ordinal positions (1 and 5) with different fingers (*Finger Specificity Control*: 2-1-3-4-2, 1-4-2-3-1 and 2-3-1-4-2) and multiple index finger keypresses occurring at alternative ordinal positions (*Position Specificity Control*: 4-2-4-3-1 and 1-4-3-4-2) **(Figure 5C)**.

Discussion

The main findings of this study were that individual sequence action representations differentiate during early skill learning in a manner reflecting the local sequence context in which they are performed, and that the degree of representational differentiation, particularly prominent during rest intervals, predicts skill gains.

Optimizing decoding of sequential finger movements from MEG activity

The initial phase of this study involved optimizing the accuracy of decoding individuated finger keypresses from MEG brain activity. The decoding of individual finger movement execution or intention is a fundamental component of many translational BCI applications[21–25]. For example, decoding of virtual keypresses can be interfaced with applications for controlling motorized wheelchairs, writing, and sending emails, or even controlling robotic hands or exoskeletons[26], and are currently being evaluated in patients with spinal cord and brain lesions[27,28]. Once these neural signals are characterized, they can be translated into meaningful commands or actions[26,29]. However, achieving robustness in clinical applications necessitates enhancements in state-of-the-art decoding tools, with a particular focus on improving decoding accuracy[23,25,30].

In the present study, we developed a novel hybrid-space decoder that captured the evolving neural representational dynamics over multiple spatial resolutions. This approach combined (1) parcel-space estimates from whole-brain activity and (2) voxel-space estimates from brain regions containing most keypress-related brain activity (see **Methods**). Using this approach, we achieved keypress state decoding accuracy that exceeded 90%, a substantial improvement over accuracies reported before with either non-invasive neuroimaging (i.e. – 43% to 77% for fMRI, MEG, and EEG)[6,23,31–33] or invasive neural recording decoding of imagined movements (i.e. – 77% to 86%

for ECOG and micro-array implant)[34,35] techniques. Given these findings, the improvement in the keypress decoding accuracy from **Figure 2** (parcel/voxel) to **Figure 3** (parcel/voxel/hybrid with dimension reduction) is likely explained by the capability of the hybrid-space architecture to capture both lower spatially resolved whole-brain and higher spatially resolved regional activity patterns that contribute unique skill-related information to the sequence-embedded keypress state representations[36]. This approach is reminiscent of the construction of convolutional neural networks (CNNs) used to perform object recognition in image classification applications[37]. It could also be view as a spatial analogue to common time-frequency based analyses such as theta-gamma phase amplitude coupling (θ/γ PAC), which assess interactions between two or more narrow-band spectral features derived from the same time-series data[38]. Importantly, this approach allowed accurate decoding during skill acquisition before a performance plateau was reached. It is possible that the ability to decode finger movements in the midst of substantial trial-by-trial performance changes as shown here could improve robustness of BCI applications in neurorehabilitation[22,39]. Accurate estimation of finger movement representations as they evolve during skill learning should also improve detection of neural replay events during wakeful rest or sleep and enhance investigations of the role replay has in supporting skill consolidation[6].

Best decoding performance was obtained from activity in the bilateral superior and middle frontal cortex and the pre- and post-central regions, all known contributors to skill learning[18,40]. The contribution of contralateral primary sensorimotor areas to early skill learning has been extensively reported in humans and non-human animals[6,12,41,42]. Similarly, the involvement of bilateral brain regions to decoding during skill learning of the left hand is not surprising. First, learning with the non-dominant left hand engages substantially more bilateral neural resources than with the dominant hand[43,44] Second, bilateral activation in both frontal and parietal cortices has been

extensively reported as essential during skill learning[45–50]. The frontal lobe is crucial for executive control[50], motor planning[46] , and working memory[45,46,51], while the parietal lobe integrates sensory feedback and visuomotor coordination[45,46,51–53], but has been also involved in working memory[54]. Thus, it is not surprising that these regions increasingly contribute to decoding as subjects internalize the sequential task.

Low-frequency oscillations (LFOs) contributed the most to decoding accuracy, consistent with previous reports[14,55]. LFOs, present during movement onset in the cerebral cortex of animals[56,57] and humans[58–60], encode information about movement trajectories and velocity[56,57]. They also contain information related to movement timing[61–63], preparation[64,65], sensorimotor integration[59], kinematics[64,65] and may contribute to the precise temporal coordination of movements required for sequencing[66]. Within clinical contexts, LFOs in the frontoparietal regions that were the main contributors to decoding performance in the present study are related to recovery of motor function after brain lesions like stroke[58,61,67,68]. Our results, in conjunction with those discussed above, suggest that LFOs contain crucial information relevant to decoding of sequence-embedded skill actions.

Neural representations of individual sequence actions are contextualized during early skill learning.

Previous work decoded actions from human neural activity when performed in isolation (e.g. individuated finger movement decoding)[14,31,32,34,35,69–72] or embedded within previously learned sequences[33,73] near stable plateau performance. To our knowledge, decoding of individual sequence-embedded actions has not been either attempted or reported within the context of rapid performance improvements that characterize early skill learning. We addressed this gap in

knowledge by investigating different decoding strategies and identified the approach that rendered the best decoding performance, which in this case was approximately 94% (5-class hybrid-space decoder). We then applied this strategy to investigate neural representations of sequential individual finger movements during the skill learning task. We found that improved 5-class decoding accuracy was linked to trial-by-trial increases in the differentiation between index finger keypresses embedded within the sequence at two different locations throughout early learning (**Figure 4C**), which occurred in parallel to skill performance improvements. Feature importance scores are initially led by the pre-central cortex during early learning followed by an intermediate shift towards post-central cortex by trial 11, which is consistent with the known role of the sensorimotor cortex in early skill acquisition[12]. Concurrently, the superior frontal and then middle frontal cortex continue to increase in importance over the Day 1 Training session and represent the two most important features between trials 15 and 36 after the rapid initial performance gains stabilize (**Figure 4 – figure supplement 1)**. This is consistent with previous findings that activity patterns within these regions represent hierarchical structures of skill sequences[16].

Neural representations are modified by experience and practice[40]. For example, FMRI studies showed that weeks-long practice of a keyboard task results in representational changes of the skill (finger sequence), but not of the individual sequence action components (individual finger movements) in the primary motor cortex[16]. An MEG study showed that previously learned individual sequence-embedded action (i.e. – finger movement) representations display an ordered queuing gradient when preparing to generate a previously learned sequence[33]. Thus, representations of previously learned skills following prolonged practice over days and weeks appear to reflect some combination of invariant features of individual action components with higher order representations of the action sequence.

Less is known about changes in neural representations during rapid performance improvements that characterize early skill learning. MEG, which possesses millisecond temporal resolution, is the tool of choice to investigate this short early learning phase[74]. In the present study, we leveraged this feature of MEG to investigate if the representation of the same sequence action (index finger movement) differentiates over early learning when embedded at different ordinal locations within the sequence. We found that practice led to a progressive differentiation of the neural representation of index finger movements reflecting the different contextual positions within the sequence. The finding that the magnitude of representational differentiation predicts skill gains supports the view that contextualization of neural representations contributes to early learning. Further support for this view comes from the finding that adding context information to the decoding algorithm increased decoding accuracy to levels higher than previously reported[14,31–35,69–73]. A possible neural mechanism supporting contextualization could be the emergence of conjunctive "what–where" representations of procedural memories[75] with the corresponding modulation of neuronal population dynamics[76,77].

Representational contextualization developed predominantly during rest periods of early learning.

Early learning defined as the period of practice that encompasses 95% of the maximal skill reached on an initial training session[1] is characterized by rapid and prominent performance improvements[1].Using a protocol that minimizes reactive inhibition effects[78], learning develops predominantly over periods of rest (micro-offline learning)[1,79,80]. Retroactive interference immediately following practice periods reduces micro-offline learning indicating stabilization of the motor memory at a scale of seconds[5], consistent with a form of rapid consolidation[5,7,80,81]. Supporting this interpretation, hippocampo-neocortical neural replay explains micro-offline

learning[6] and human hippocampal ripples during rest intervals, known markers of neural replay, predict micro-offline as well as total learning[10,82]. Three lines of evidence suggest that micro-offline gains during early learning are not a result of recovery from motor fatigue. First, we used a protocol already reported to minimize reactive inhibition effects (Pan and Rickard recommended this approach because "*…rapid learning during that period masks any reactive inhibition effect"*[78]). Second, micro-offline learning is unaffected by shortening in half practice intervals' duration and thus hypothetical fatigue[5]. Finally, learning faster, more fatiguing, skills reduce instead of enhance micro-offline learning[97].

Representational contextualization during early learning developed to a larger extent during rest than during practice. Importantly, within-subject correlations for contextualization changes during rest intervals and micro-offline gains were significantly higher than between online contextualization and micro-online gains or between online contextualization and micro-offline gains (**Figure 5 – figure supplement 4**). Together with the observation that rapid contextualization was retained the following day, reflecting stability of the skill memory over time, and in line with previous work[1,83], our findings suggest that contextualization of action representations contribute to early skill learning, particularly during rest intervals.

Representational contextualization after early learning.

The magnitude of contextualization stabilized after early learning. The rapid initial skill gains that characterize early learning are followed by micro-scale fluctuations around skill plateau levels (i.e. following trial 11 in **Figure 1B**). These fluctuations (i.e. - micro-online drops and micro-offline rebounds in the absence of net skill gains) have been attributed to reactive inhibition mechanisms[1,84]. Similar fluctuations are observed in non-learning contexts, for example when performing non-repeating sequences [85]. Thus, the mechanisms underlying micro-scale changes

differ between early learning and after plateau skill has been reached[1,84]. Evaluation of micro-offline gains within training contexts where reactive inhibition is prominent (e.g. - after early learning or when performing non-repeating sequences[85–87]) or testing during time intervals within which post-learning consolidation, interference or forgetting may occur[85] confounds early learning measurements[1,78]. Similarly, utilizing the initial practice trials (during which about 40-50% of early learning occurs[1]) as "tests" before introducing practice schedule interventions amputates early learning almost in half, markedly distorting its measurement[85]. Our data suggest that contextualization within an initial training session does not improve further after early skill learning.

Limitations

One limitation of this study is that contextualization was investigated for only one finger movement (index finger or digit 4) embedded within a relatively short 5-item skill sequence. It will be useful to find out if representational contextualization of multiple finger movements embedded within longer sequences (e.g. – a short piece of piano music) exhibit similar results. The use of a supervised manifold learning approach (LDA) in this study could be improved in the future by implementing unsupervised strategies more suitable for real-time BCI applications (e.g. - PCA and MDS also substantially improved decoding accuracy in the present study; **Figure 3 – figure supplement 2**). Finally, caution should be used when extrapolating findings during early skill learning to post-plateau performance periods, longer practice timespans, or non-learning situations (e.g. on-repeating groups in[85]) when reactive inhibition plays a more substantive role. Ultimately, it will be important to develop new paradigms allowing one to independently estimate the different coincident or antagonistic features (e.g. - memory consolidation, planning, working

memory and reactive inhibition) contributing to micro-online and micro-offline gains during and after early skill learning within a unifying framework.

Summary

In summary, individual sequence action representations contextualize during the initial practice trials of a new skill and the degree of differentiation parallels skill gains. Importantly, the offline neural representational change develops to a larger extent during rest than during practice intervals of early learning in parallel with rapid consolidation of skill. It is possible that the systematic inclusion of contextualized information into sequence skill practice environments could improve learning in areas as diverse as music education, sports training, and rehabilitation of motor skills after brain lesions.

Materials and Methods

Study Participants

The study was approved by the Combined Neuroscience Institutional Review Board of the National Institutes of Health (NIH). A total of thirty-three young and healthy adults (comprising 16 females) with a mean age of 26.6 years (± 0.87 SEM) participated in the study after providing written informed consent and undergoing a standard neurological examination. No participants were actively engaged in playing musical instruments in their daily lives, as per guidelines outlined in prior research[88,89]. All study scientific data were de-identified and permanently unlinked from all personal identifiable information (PII) before the analysis. These data are publicly available upon request (https://nih.box.com/v/hcpsSkillLearningData). Two participants were excluded from the analysis due to MEG system malfunction during data acquisition. An additional 5 subjects were excluded because they failed to generate any correct sequences in two or more consecutive

trials. The study was powered to determine the minimum sample size needed to detect a significant change in skill performance following training using a one-sample t-test (two-sided; alpha = 0.05; 95% statistical power; Cohen's d effect size = 0.8115 calculated from previously acquired data in our lab[90]). The calculated minimum sample size was 22. The included study sample size (n = 27) exceeded this minimum. [1]

Experimental Setup

Participants practiced a novel procedural motor skill learning task that involved repetitively typing a 5-item numerical sequence (4-1-3-2-4) displayed on a computer screen. They were instructed to perform the task as quickly and accurately as possible using their non-dominant, left hand on a response pad (Cedrus LS-LINE, Cedrus Corp). Each numbered sequence item corresponded to a specific finger keypress: 1 for a little finger keypress, 2 for a ring finger keypress, 3 for a middle finger keypress, and 4 for an index finger keypress. Individual keypress times and identities were recorded and used to assess skill learning and performance.

Participants practiced the skill for 36 trials. Each trial spanned a total of 20 seconds and included a 10 second practice round followed by a 10 second inter-practice rest period. The five-item sequence was displayed on the computer screen for the duration of each practice round and participants were directed to fix their gaze on the sequence. Small asterisks were displayed above a sequence item after each successive keypress, signaling the participants' present position within the sequence. Following the completion of a full sequence iteration, the asterisks were removed. The asterisk display did not provide error feedback as it appeared for both correct and incorrect keypresses. At the end of each practice round, the displayed number sequence was replaced by a string of five "X" symbols displayed on the computer screen, which remained for the duration of the inter-practice rest period. Participants were instructed to focus their gaze on the screen during

this time. The behavior in this explicit sequence learning motor tasks is highly generative in nature rather than reactive to stimulus cues as in the serial reaction time task (SRTT). A similar real-world example would be manually inputting a long password into a secure online application in which one intrinsically generates the sequence from memory and receives similar feedback about the password sequence position (also provided as asterisks), which is typically ignored by the user.

On the next day, participants were tested (*Day 2 Retest*) with the same trained sequence (4-1-3-2-4) for 9 trials as well as for 9 different unpracticed control sequences (*Day 2 Control*; 2-1-3-4-2; 4-2-4-3-1; 3-4-2-3-1; 1-4-3-4-2; 3-2-4-3-1; 1-4-2-3-1; 3-2-4-2-1; 2-3-1-4-2; 4-2-3-1-4) each for one trial. The practice schedule structure for Day 2 was same as Day 1, with 10s practice trials interleaved with 10s of rest.

Behavioral data analysis

Skill

Skill, in the context of the present task, is quantified as the *correct sequence typing speed*, (i.e., - the number of correctly typed sequence keypresses per second; kp/s). That is, improvements in the speed/accuracy trade-off equate to greater skill. Keypress transition times (KTT) were calculated as the difference in time between the *keyDown* events recorded for consecutive keypresses. Since the sequence was repeatedly typed within a single trial, individual keypresses were marked as correct if they were members of a 5 consecutive keypress set that matched any possible circular shift of the displayed 5-item sequence. The instantaneous correct sequence speed was calculated as the inverse of the average KTT across a single correct sequence iteration and was updated for each correct keypress. Trial-by-trial skill changes were assessed by computing the median correct sequence typing speed for each trial.

Early Learning

The *early learning* period was defined as the trial range (1 - T trials) over which 95% of the total skill performance was first attained at the group level. We quantified this by fitting the group average trial-by-trial correct sequence speed data with an exponential model of the form:

$$L(t) = C1 + C2\,(1 - e^{-kt})$$

Here, the trial number is denoted by *t*, and *L(t)* signifies the group-averaged performance at trial *t*. Parameters *C1* and *C2* correspond to the pre-training performance baseline and asymptote, respectively, while *k* denotes the learning rate. The values for *C1*, *C2*, and *k* were computed using a constrained nonlinear least-squares method (MATLAB's lsqcurvefit function, trust-region-reflective algorithm) and were determined to be 0.5, 0.15, and 0.2, respectively. The early learning trial cut-off, denoted as *T*, was identified as the first trial where 95% of the learning had been achieved. In this study, *T* was determined to be trial 11.

Performance improvements during rest (*micro-offline gains)*, for each rest period of a trial, were calculated as the net change in performance (instantaneous correct sequence typing speed) from the end of one practice period to the onset of the next (i.e. – over a single inter-practice rest period). *Micro-online gains* (performance improvements during practice periods) were computed as the change in performance between the beginning and end of a single practice trial. Total early learning was derived as the sum of all *micro-online* and *micro-offline* gains over trials 1-11. Cumulative micro-offline gains, micro-online gains, and total early learning were statistically compared using 1-way ANOVAs and post-hoc Tukey tests.

MRI Acquisition

We acquired T1-weighted high-resolution anatomical MRI volumes images (1 mm^3 isotropic MPRAGE sequence) for each participant on a 3T MRI scanner (GE Excite HDxt or Siemens Skyra) equipped with a 32-channel head coil. These data allowed for spatial co-registration of an individual participant's brain with the MEG sensors, and individual head models required for surface-based cortical dipole estimation from MEG signals (i.e. – MEG source-space modeling).

MEG Acquisition

We recorded continuous magnetoencephalography (MEG) at a sampling frequency of 600 Hz using a CTF 275 MEG system (CTF Systems, Inc., Canada) while participants were seated in an upright position. The MEG system comprises a whole-head array featuring 275 radial 1st-order gradiometer/SQUID channels housed in a magnetically shielded room (Vacuumschmelze, Germany). Three of the gradiometers (two non-functional and one with high channel noise after visual inspection) were excluded from the analysis resulting in a total of 272 MEG channels for analysis. Synthetic 3rd order gradient balancing was applied to eliminate background noise in real-time data collection. Temporal alignment of behavioral and MEG data was achieved using a TTL trigger. Head position in the scanner coordinate space was monitored using head localization coils at the nasion, left, and right pre-auricular locations. These fiducial positions were co-registered in the participants' T1-MRI coordinate space using a stereotactic neuronavigation system (BrainSight, Rogue Research Inc.). MEG data was acquired starting 6 min before the task (resting-state baseline) and continued through the end of the 12 min training session.

MEG Data Analysis

Preprocessing

MEG data were preprocessed using the FieldTrip[91] and EEGLAB[92] toolboxes on MATLAB 2022a. Continuous raw MEG data (acquired at 600 Hz) were band-pass filtered between 1-100 Hz with a 4th order noncausal Butterworth filter. 60 Hz line noise was removed with a narrow-band discrete Fourier transform (DFT) notch filter. Independent component analysis (ICA) was used to remove typical MEG signal artifacts related to eye blinks or movement or cardiac pulsation. All recordings were visually inspected and marked to denoise segments containing other large amplitude artifacts due to movements.

Source Reconstruction and Parcellation

For each participant, individual volume conduction models were established to depict the propagation of brain-generated currents through tissue to externally measurable magnetic fields. This was accomplished through a single-shell head corrected-sphere approach based on the brain volume segmentation of their high-resolution T1 MRI. Source models and surface labels from the Desikan-Killiany Atlas[19] were created for each participant using inner-skull and pial layer surfaces obtained through FreeSurfer segmentation and connectome-workbench. Aligning sensor positions in the MEG helmet to individual head space involved warping MEG head coil positions (mean of pre and post recording) to the fiducials of the MRI, applying the same transformation matrix to all MEG sensors.

The individual source, volume conduction model, and sensor positions were then utilized to generate the forward solution at each source dipole location, describing the propagation of source activity from each cortical location on the grid to each MEG sensor. The Linearly Constrained Minimum-Variance (LCMV) beamformer was employed for computing the inverse solution. Each

trial of MEG activity contributed to calculating the inverse solution data covariance matrix. The individual sample noise covariance matrix was derived from 6 minutes of pre-training rest MEG data recorded in the same subject during the same session. A total of 15,684 surface-based cortical dipoles (source-space voxels) were estimated. Cortical parcellation involved averaging the time series of all source dipoles within a distinct anatomical boundary defined in the Desikan-Killiany Atlas. To prevent within-parcel source cancellation during averaging, a technique called mean-flipping was applied. This process entailed flipping the sign for all sources with a sign differing from that of the average source.

Feature Selection for Decoding

Features were extracted from the MEG activity at several spatial, oscillatory, and temporal scales.

Oscillatory Analysis

MEG signals were band limited to broadband (1-100 Hz) and standard neural oscillatory frequency bands defined as delta (1-3 Hz), theta (4-7 Hz), alpha (8-14 Hz), beta (15-24 Hz), gamma (25-50 Hz), and high-gamma (51-100 Hz) with a 4th order non-causal Butterworth filter. The decoding analysis was conducted independently for each band of MEG activity.

Spatial Analysis.

Decoding was performed at sensor space as well as at source space. For sensor space decoding the feature dimension was 272 (corresponding to the 272 gradiometer channels). At the source space, decoding was executed at both the high-resolution voxel and low-resolution parcel space. The feature dimension for voxel-space decoding was 15,684, representing the total number of independently estimated cortical dipoles. For parcel-space decoding, the feature dimension was 148, derived from spatially averaging the voxel activities within each parcel defined by the Desikan-Killiany Atlas. In both cases, decoding was carried out across all oscillatory frequency

bands (i.e. - broadband, delta, theta, alpha, beta, gamma, and high-gamma) for comprehensive comparison.

Temporal Analysis.

Temporal MEG activity corresponding to each keypress was defined by taking a time window of [t + Δt], where t ∈ [0 : 10 ms : 100 ms] and Δt ∈ [25 ms : 25 ms : 350 ms]. In other words, a sliding window of variable width (from 25 ms to 350 ms with 25 ms increments) with onset ranging from the *keyDown* event (i.e. – t = 0ms) to +100ms after the *keyDown* event (with increments of 10 ms) was used. This approach generated 140 different temporal windows for each keypress for each participant. MEG activity was averaged over each of these time widows and independently analyzed for decoding. The optimal time window was selected for each subject that resulted in best cross-validation performance (**Figure 4 – figure supplement 2**). This window optimization analysis was performed for each frequency band and spatial scale.

Hybrid Spatial Approach.

First, we evaluated the decoding performance of each brain region in decoding finger identity. We trained decoders on the voxel activities of each region (intra-parcel decoders) to predict finger identity. Brain regions were then ranked from 1 to 148 based on their decoding accuracy at the group level. In a stepwise manner, we incrementally incorporated voxel activities of brain regions, starting from the top-ranked region. In other words, first, we concatenated the voxel-level features of the highest-ranked region with whole-brain parcel-level features for decoding analysis. Subsequently, we added the voxel-level features of the second-ranked brain region, along with those of the top-ranked region to the parcel-level features for decoding and continued this process. This iterative addition of brain regions was performed until decoding accuracy reached saturation.

The optimal feature space comprised all 148 parcel-space features in conjunction with voxel-space features from the top 8 brain regions.

Dimension Reduction

We used several supervised and unsupervised dimension reduction techniques including linear discriminant analysis (LDA), minimum redundant maximum relevance (MRMR), principal component analysis (PCA), Autoencoder, Diffusion maps, factor analysis, large margin nearest neighbor (LMNN), multi-dimensional scaling (MDS), neighbor component analysis (NCA), spatial predictor envelope (SPE)[20] on each of the spatial feature space (sensor, parcel, voxel, and hybrid). Among these techniques, PCA, MDS, MRMR, and LDA emerged as particularly effective in significantly improving decoding performance.

PCA, a method for unsupervised dimensionality reduction, transformed the high-dimensional dataset into a new coordinate system of uncorrelated principal components. These components, capturing the maximum variance in the data, were iteratively added to reconstruct the feature space and execution of decoding. MDS finds a configuration of points in a lower-dimensional space such that the distances between these points reflect the dissimilarities or similarities between the corresponding objects in the original high-dimensional space. MRMR, an approach combining relevance and redundancy metrics, ranked features based on their significance to the target variable and their non-redundancy with other features. The decoding process involved starting with the highest-ranked feature and iteratively incorporating subsequent features until decoding accuracy reached saturation. LDA finds the linear combinations of features (dimensions) that best separate different classes in a dataset. It projects the original features onto a lower-dimensional space (number of classes -1) while preserving the class-discriminatory information. This transformation maximizes the ratio of the between-class variance to the within-class variance. In our study, LDA

transformed the features to a 3-dimensional hyperdimensional space that were used for decoding. Dimension reduction was applied to train data and then with the tuned parameters of the dimension reduction model test data was transformed for decoder metrics evaluation. Decoding accuracies were systematically compared between the original and reduced dimension feature spaces, providing insights into the effectiveness of each dimension reduction technique. By rigorously assessing the impact of dimension reduction on decoding accuracy, the study aimed to identify techniques that not only reduced the computational burden associated with high-dimensional data but also enhanced the discriminative power of the selected features. This comprehensive approach aimed at optimizing the neural representation of each finger keypress for decoding performance across various spatial contexts.

Decoding Analysis

Decoding analysis was conducted for each participant individually, employing a randomized split of the data into training (90%) and test (10%) samples for 8 iterations. For each iteration, to optimize decoder configuration, an 8-fold cross-validation was applied to the training samples, allowing for the fine-tuning of hyperparameters and selection of the most effective model. Across participants, on average, the total number of individual keypresses for the whole duration of training was 219 ± SD: 66 (keypress 1: little), 205 ± SD: 66 (keypress 2: ring), 209 ± 66 (keypress 3: middle), and 426 ± SD: 131 (keypress 4: index). Only keypresses belonging to correctly typed sequence iterations (94.64% ± 4.04% of all keypresses) were considered. The total number of keypresses for keypress 4 was approximately twice that of keypresses 1, 2, and 3, as it was the only action that occurred more than once in the trained sequence (4-1-3-2-4), albeit in two different sequence contexts or ordinal positions. Considering the higher (2x) number of samples for one-class, we independently oversampled the keypresses 1, 2 and 3 to avoid overfitting to the over-

represented class. Importantly, oversampling was applied independently for each keypress class, ensuring that validation folds were never oversampled, and training folds did not share common oversampled patterns. The decoder configuration demonstrating the best validation performance was selected for each iteration, and subsequently, test accuracy was evaluated on the independent/unseen test samples. This process was repeated for the 8 different iterations of train-test splitting and the average test accuracy was reported. This rigorous methodology aimed at generalizing decoding performance to ensure robust and reliable results across participants. Further, decoding evaluation was performed on the Day 2 data, for both the trained (*Day 2 Retest;* 9 trials) and untrained sequences (*Day 2 Control*; 9 different single-trial tests).

Machine Learning Classifiers

We employed a diverse set of machine learning decoders, including Naïve Bayes (NB), decision trees (DT), ensembles (EN), k-nearest neighbor (KNN), linear discriminant analysis (LDA), support vector machines (SVM), and artificial neural network (ANN), to train features generated with all possible combinations of spatial, temporal, and oscillatory scales for comprehensive comparative analysis. The hyperparameters of these decoders underwent fine-tuning using Bayesian optimization search.

The Naive Bayes classifier was configured with a normal distribution predictor and Gaussian Kernel, while the KNN classifier had a K value of 4 (for keypress decoding) and utilized the Euclidean distance metric. For decision trees, the maximum number of splits was set to 4 (for keypress decoding), with leaves being merged based on the sum of risk values greater or equal to the risk associated with the parent node. The optimal sequence of pruned trees was estimated, and the predictor selection method was 'Standard CART,' selecting the split predictor that maximizes the split-criterion gain over all possible splits of all predictors. The split criterion used was 'gdi'

(Gini's diversity index). Ensembles employed the bagging method with random predictor selections at each split, forming a random forest. The maximum number of learning cycles was set to 100 with a weak learner based on discriminant analysis. For SVM, the RBF kernel was selected through cross-validation (CV), and the 'C' parameter and kernel scale were optimized using Bayesian optimization search. In the case of LDA, the linear coefficient threshold and the amount of regularization were computed based on Bayesian optimization search. The ANN decoder consisted of one hidden layer with 128 nodes, followed by a sigmoid and a softmax layer, each with 4 nodes (for keypress decoding). Training utilized a scaled conjugate gradient optimizer with backpropagation, employing a learning rate of 0.01 (coarse to fine tuning) for a maximum of 100 epochs, with early stopping validation patience set to 6 epochs.

Additionally, we assessed long short-term memory recurrent neural networks (LSTM-RNN) and bidirectional LSTM-RNN to train the time series of each keypress for decoding. The configuration of these RNNs included two hidden (Bi)LSTM layers of 100 units, followed by three fully connected layers (50, 10, and 4), and a softmax layer with 4 nodes to decode the four keypress classes. The networks were trained using an Adam optimizer with an initial learning rate of 0.001, a learning rate drop factor of 0.1 after 20 epochs, and a maximum epoch of 400. For regularization, 20% dropouts after the (Bi)LSTM layers, 50% dropout after the fully connected layers, and L2 Norm with a gradient threshold value of 0.1 were employed. These hyperparameter values were chosen based on grid search optimization during cross-validation.

Decoding Performance Metrics

Decoding performance was assessed using several metrics, including accuracy (%), which indicates the proportion of correct classifications among all test samples. The confusion matrix provided a detailed comparison of the number of correctly predicted samples for each class against

the ground truth. The F1 score, defined as the harmonic mean of the precision (percentage of true predictions that are actually true positive) and recall (percentage of true positives that were correctly predicted as true) scores, was used as a comprehensive metric for all one-versus-all keypress state decoders to assess class-wise performance that accounts for both false-positive and false-negative prediction tendencies[93,94]. A weighted mean F1 score was then computed across all classes to assess the overall prediction performance of the multi-class model. Test accuracies based on the best decoder performance (LDA in our case) were reported and used for statistical comparisons.

Decoding During Skill Learning Progression

We systematically assessed decoding performance of the 2-class decoder ($\text{Index}_{\text{OP1}}$ vs $\text{Index}_{\text{OP5}}$) at each trial during the skill learning process to identify the relationship between the evolution of differentiated index finger decoding proficiency and the acquired skill. Our approach involved evaluating decoder performance individually for each *Day 1 Training* trial. To mitigate the influence of varying sample sizes in later trials, we ensured an equal number of samples (first *k* keypresses) in each trial.

We used t-distributed stochastic neighborhood estimation (t-SNE) to visualize the evolution of neural representations corresponding to each keypress at each trial of the learning period. Within t-SNE distributions, index finger keypresses were separately labeled based upon their sequence location (i.e., $\text{Index}_{\text{OP1}}$ and $\text{Index}_{\text{OP5}}$ for ordinal positions 1 and 5, respectively).

Decoding Sequence Elements

Finally, we performed decoding of each contextual action of the sequence (i.e., $\text{Index}_{\text{OP1}}$, Little, Middle, Ring, and $\text{Index}_{\text{OP5}}$). We used the same decoding strategy (90%-10% split for train and test, 8-fold cross validation of training samples to select best decoder configuration, hybrid spatial

features, and LDA based dimension reduction) to decode these 5-classes. Note, oversampling was not needed after sub-grouping the index finger keypresses into two separate classes based on their context. Decoding sequence elements were evaluated for both *Day 1 Training*, *Day 2 Retest* and *Day 2 Control* data.

Feature Importance Scores

The relative contribution of source-space voxels and parcels to decoding performance (i.e. – feature importance score) was calculated using minimum redundant maximum relevance (MRMR)[95] and highlighted in topography plots. MRMR, an approach that combines both relevance and redundancy metrics, ranked individual features based upon their significance to the target variable (i.e. – keypress state identity) prediction accuracy and their non-redundancy with other features.

Neural Representation analysis

We evaluated the *online* (within-trial) and *offline* (between-trial) changes in the neural representation of the contextual actions (Index_{OP1} and Index_{OP5}) for each trial during training. For offline differentiation, we evaluated the Euclidian distance between the hybrid spatial features of the last index finger keypress of a trial (Index_{OP5}) to the first index finger keypress (Index_{OP1}) of the subsequent trial, mirroring the approach used to calculate micro-offline gains in skill. This offline distance provided insights on the net change in contextual representation of the index finger keypress during each interspersed rest interval. For online differentiation, we calculated the mean Euclidian distance between Index_{OP1} and Index_{OP5} of all the correctly typed sequences within a practice trial. Online differentiation informed on the net change in the contextual representation of the index finger keypress within each practice trial. Cumulative offline and online representation distances across participants were compared using 2-sample *t*-tests. Additionally, we computed

trial-by-trial differences in offline and online representations during early learning, exploring their relationships with cumulative micro-offline and micro-online gains in skill, respectively, through regression analysis and Pearson correlation analysis. Linear regression models were trained utilizing the *fitlm* function in MATLAB. The model employed M-estimation, formulating estimating equations and solving them through the Iteratively Reweighted Least Squares (IRLS) method[96]. Key metrics such as the square root of the mean squared error (RMSE), which estimates the standard deviation of the prediction error distribution, the coefficient of explained variance (R^2), the F-statistic as a test statistic for the F-test on the regression model, examining whether the model significantly outperforms a degenerate model consisting only of a constant term, and the *p*-value for the F-test on the model were computed and compared across different models. This multifaceted approach aimed to uncover the nuanced dynamics of neural representation changes in response to skill acquisition.

As a control analysis, we also computed the difference in neural representation between $\text{Index}_{\text{OP1}}$ and $\text{Index}_{\text{OP5}}$ on *Day 2 Retest* data for the same sequence (**4**-1-3-2-**4**) as well as for different *Day 2 Control* untrained sequences where the same action was performed at ordinal positions 1 and 5 (**2**-1-3-4-**2**; **1**-4-2-3-**1**; **2**-3-1-4-**2**; **4**-2-3-1-**4**). Finally, we assessed for specificity of contextualization to the trained sequence, by evaluating differentiation between index finger keypress representations performed at two different positions within untrained sequences (**4**-2-**4**-3-1 and 1-**4**-3-**4**-2). The cumulative differences across participants were compared with 2-sample *t*-tests.

Data Availability

All de-identified and permanently unlinked from all personal identifiable information (PII) data are publicly available. (Box Repository).

Acknowledgments.

We thank Ms. Tasneem Malik, Ms. Michele Richman, and NIMH MEG Core Facility staff for their support. This work utilized the computational resources of the NIH HPC Biowulf cluster (http://hpc.nih.gov). This research was supported by the Intramural Research Program of the NINDS, NIH.

REFERENCES

1. Bönstrup, M. *et al.* A rapid form of offline consolidation in skill learning. *Current Biology* **29**, 1346–1351 (2019).

2. Schmidt, R. A., Lee, T. D., Winstein, C., Wulf, G. & Zelaznik, H. N. *Motor Control and Learning: A Behavioral Emphasis*. (Human kinetics, 2018).

3. Doyon, J. & Benali, H. Reorganization, and plasticity in the adult brain during learning of motor skills. *Curr Opin Neurobiol* **15**, 161–167 (2005).

4. Dehaene, S., Meyniel, F., Wacongne, C., Wang, L. & Pallier, C. The neural representation of sequences: from transition probabilities to algebraic patterns and linguistic trees. *Neuron* **88**, 2–19 (2015).

5. Bönstrup, M., Iturrate, I., Hebart, M. N., Censor, N. & Cohen, L. G. Mechanisms of offline motor learning at a microscale of seconds in large-scale crowdsourced data. *NPJ Sci Learn* **5**, 1–10 (2020).

6. Buch, E. R., Claudino, L., Quentin, R., Bönstrup, M. & Cohen, L. G. Consolidation of human skill linked to waking hippocampo-neocortical replay. *Cell Rep* **35**, 109193 (2021).

7. Jacobacci, F. *et al.* Rapid hippocampal plasticity supports motor sequence learning. *Proceedings of the National Academy of Sciences* **117**, 23898–23903 (2020).

8. Deleglise, A. *et al.* Human motor sequence learning drives transient changes in network topology and hippocampal connectivity early during memory consolidation. *Cerebral Cortex* **33**, 6120–6131 (2023).

9. Chen, S. & Epps, J. Using task-induced pupil diameter and blink rate to infer cognitive load. *Hum Comput Interact* **29**, 390–413 (2014).

10. Sjøgård, M. *et al.* Hippocampal ripples mediate motor learning during brief rest breaks in humans. *bioRxiv* 2024–2025 (2024).

11. Buzsáki, G. Hippocampal sharp wave-ripple: A cognitive biomarker for episodic memory and planning. *Hippocampus* **25**, 1073–1188 (2015).

12. Kami, A. *et al.* Functional MRI evidence for adult motor cortex plasticity during motor skill learning. *Nature* **377**, 155–158 (1995).

13. Song, S. & Cohen, L. G. Practice and sleep form different aspects of skill. *Nat Commun* **5**, 3407 (2014).

14. Natraj, N., Silversmith, D. B., Chang, E. F. & Ganguly, K. Compartmentalized dynamics within a common multi-area mesoscale manifold represent a repertoire of human hand movements. *Neuron* **110**, 154–174 (2022).

15. Ghilardi, M. F., Moisello, C., Silvestri, G., Ghez, C. & Krakauer, J. W. Learning of a sequential motor skill comprises explicit and implicit components that consolidate differently. *J Neurophysiol* **101**, 2218–2229 (2009).

16. Yokoi, A. & Diedrichsen, J. Neural organization of hierarchical motor sequence representations in the human neocortex. *Neuron* **103**, 1178–1190 (2019).

17. Beukema, P., Diedrichsen, J. & Verstynen, T. D. Binding during sequence learning does not alter cortical representations of individual actions. *Journal of Neuroscience* **39**, 6968–6977 (2019).

18. Hikosaka, O. *et al.* Parallel neural networks for learning sequential procedures. *Trends Neurosci* **22**, 464–471 (1999).

19. Destrieux, C., Fischl, B., Dale, A. & Halgren, E. Automatic parcellation of human cortical gyri and sulci using standard anatomical nomenclature. *Neuroimage* **53**, 1–15 (2010).

20. Van Der Maaten, L., Postma, E. O. & van den Herik, H. J. Dimensionality reduction: A comparative review. *Journal of Machine Learning Research* **10**, 13 (2009).

21. Merino, E. C., Faes, A. & Van Hulle, M. M. The role of distinct ECoG frequency features in decoding finger movement. *J Neural Eng* **20**, 066014 (2023).

22. Liu, C. *et al.* Decoding the EEG patterns induced by sequential finger movement for brain-computer interfaces. *Front Neurosci* **17**, (2023).

23. Lee, H. S. *et al.* Individual finger movement decoding using a novel ultra-high-density electroencephalography-based brain-computer interface system. *Front Neurosci* **16**, 1009878 (2022).

24. Zhao, Y. *et al.* Decoding finger movement patterns from microscopic neural drive information based on deep learning. *Med Eng Phys* **104**, 103797 (2022).

25. Yao, L., Zhu, B. & Shoaran, M. Fast and accurate decoding of finger movements from ECoG through Riemannian features and modern machine learning techniques. *J Neural Eng* **19**, 016037 (2022).

26. Buch, E. *et al.* Think to move: a neuromagnetic brain-computer interface (BCI) system for chronic stroke. *Stroke* **39**, 910–917 (2008).

27. Vogel, J. *et al.* Continuous control of the dlr light-weight robot iii by a human with tetraplegia using the braingate2 neural interface system. in *Experimental Robotics: The 12th International Symposium on Experimental Robotics* 125–136 (Springer, 2014).

28. Rubin, D. B. & Hochberg, L. R. BrainGate: An Intracortical Brain-Computer Interface for the Restoration of Communication and Functional Independence for People with Paralysis. in *2023 11th International Winter Conference on Brain-Computer Interface (BCI)* 1–3 (IEEE, 2023).

29. Birbaumer, N. & Cohen, L. G. Brain–computer interfaces: communication and restoration of movement in paralysis. *J Physiol* **579**, 621–636 (2007).

30. Birbaumer, N., Murguialday, A. R. & Cohen, L. Brain–computer interface in paralysis. *Curr Opin Neurol* **21**, 634–638 (2008).

31. Liao, K., Xiao, R., Gonzalez, J. & Ding, L. Decoding individual finger movements from one hand using human EEG signals. *PLoS One* **9**, e85192 (2014).

32. Quandt, F. *et al.* Single trial discrimination of individual finger movements on one hand: a combined MEG and EEG study. *Neuroimage* **59**, 3316–3324 (2012).

33. Kornysheva, K. *et al.* Neural competitive queuing of ordinal structure underlies skilled sequential action. *Neuron* **101**, 1166–1180 (2019).

34. Shenoy, P., Miller, K. J., Ojemann, J. G. & Rao, R. P. N. Finger movement classification for an electrocorticographic BCI. in *2007 3rd International IEEE/EMBS Conference on Neural Engineering* 192–195 (IEEE, 2007).

35. Onaran, I., Ince, N. F., Cetin, A. E. & Abosch, A. A hybrid SVM/HMM based system for the state detection of individual finger movements from multichannel ECoG signals. in *2011 5th International IEEE/EMBS Conference on Neural Engineering* 457–460 (IEEE, 2011).

36. Munn, B. R. *et al.* Multiscale organization of neuronal activity unifies scale-dependent theories of brain function. *Cell* (2024).

37. Srinivas, S. *et al.* A taxonomy of deep convolutional neural nets for computer vision. *Front Robot AI* **2**, 36 (2016).

38. Lisman, J. E. & Jensen, O. The theta-gamma neural code. *Neuron* **77**, 1002–1016 (2013).

39. Presacco, A., Forrester, L. W. & Contreras-Vidal, J. L. Decoding intra-limb and inter-limb kinematics during treadmill walking from scalp electroencephalographic (EEG) signals. *IEEE Transactions on neural systems and rehabilitation engineering* **20**, 212–219 (2012).

40. Dayan, E. & Cohen, L. G. Neuroplasticity subserving motor skill learning. *Neuron* **72**, 443–454 (2011).

41. Classen, J., Liepert, J., Wise, S. P., Hallett, M. & Cohen, L. G. Rapid plasticity of human cortical movement representation induced by practice. *J Neurophysiol* **79**, 1117–1123 (1998).

42. Kleim, J. A., Barbay, S. & Nudo, R. J. Functional reorganization of the rat motor cortex following motor skill learning. *J Neurophysiol* **80**, 3321–3325 (1998).

43. Sawamura, D. *et al.* Acquisition of chopstick-operation skills with the non-dominant hand and concomitant changes in brain activity. *Sci Rep* **9**, 20397 (2019).

44. Lee, S. H., Jin, S. H. & An, J. The difference in cortical activation pattern for complex motor skills: A functional near-infrared spectroscopy study. *Sci Rep* **9**, 14066 (2019).

45. Shadmehr, R. & Holcomb, H. H. Neural correlates of motor memory consolidation. *Science (1979)* **277**, 821–825 (1997).

46. Toni, I., Ramnani, N., Josephs, O., Ashburner, J. & Passingham, R. E. Learning arbitrary visuomotor associations: temporal dynamic of brain activity. *Neuroimage* **14**, 1048–1057 (2001).

47. Doyon, J. *et al.* Experience-dependent changes in cerebellar contributions to motor sequence learning. *Proceedings of the National Academy of Sciences* **99**, 1017–1022 (2002).

48. Grafton, S. T. *et al.* Functional anatomy of human procedural learning determined with regional cerebral blood flow and PET. *Journal of Neuroscience* **12**, 2542–2548 (1992).

49. Kennerley, S. W., Sakai, K. & Rushworth, M. F. S. Organization of action sequences and the role of the pre-SMA. *J Neurophysiol* **91**, 978–993 (2004).

50. Hardwick, R. M., Rottschy, C., Miall, R. C. & Eickhoff, S. B. A quantitative meta-analysis and review of motor learning in the human brain. *Neuroimage* **67**, 283–297 (2013).

51. Wolpert, D. M., Goodbody, S. J. & Husain, M. Maintaining internal representations: the role of the human superior parietal lobe. *Nat Neurosci* **1**, 529–533 (1998).

52. Andersen, R. A. & Buneo, C. A. Intentional maps in posterior parietal cortex. *Annu Rev Neurosci* **25**, 189–220 (2002).

53. Buneo, C. A. & Andersen, R. A. The posterior parietal cortex: sensorimotor interface for the planning and online control of visually guided movements. *Neuropsychologia* **44**, 2594–2606 (2006).

54. Grover, S., Wen, W., Viswanathan, V., Gill, C. T. & Reinhart, R. M. G. Long-lasting, dissociable improvements in working memory and long-term memory in older adults with repetitive neuromodulation. *Nat Neurosci* 1–10 (2022).

55. Reddy, L. *et al.* Theta-phase dependent neuronal coding during sequence learning in human single neurons. *Nat Commun* **12**, 4839 (2021).

56. Bansal, A. K., Vargas-Irwin, C. E., Truccolo, W. & Donoghue, J. P. Relationships among low-frequency local field potentials, spiking activity, and three-dimensional reach and grasp kinematics in primary motor and ventral premotor cortices. *J Neurophysiol* **105**, 1603–1619 (2011).

57. Mollazadeh, M. *et al.* Spatiotemporal variation of multiple neurophysiological signals in the primary motor cortex during dexterous reach-to-grasp movements. *Journal of Neuroscience* **31**, 15531–15543 (2011).

58. Bönstrup, M. *et al.* Low-frequency brain oscillations track motor recovery in human stroke. *Ann Neurol* **86**, 853–865 (2019).

59. Cruikshank, L. C., Singhal, A., Hueppelsheuser, M. & Caplan, J. B. Theta oscillations reflect a putative neural mechanism for human sensorimotor integration. *J Neurophysiol* **107**, 65–77 (2012).

60. Tomassini, A., Ambrogioni, L., Medendorp, W. P. & Maris, E. Theta oscillations locked to intended actions rhythmically modulate perception. *Elife* **6**, e25618 (2017).

61. Ramanathan, D. S. *et al.* Low-frequency cortical activity is a neuromodulatory target that tracks recovery after stroke. *Nat Med* **24**, 1257–1267 (2018).

62. Hall, T. M., Nazarpour, K. & Jackson, A. Real-time estimation and biofeedback of single-neuron firing rates using local field potentials. *Nat Commun* **5**, 5462 (2014).

63. Stefanics, G. *et al.* Phase entrainment of human delta oscillations can mediate the effects of expectation on reaction speed. *Journal of Neuroscience* **30**, 13578–13585 (2010).

64. Flint, R. D., Ethier, C., Oby, E. R., Miller, L. E. & Slutzky, M. W. Local field potentials allow accurate decoding of muscle activity. *J Neurophysiol* **108**, 18–24 (2012).

65. Krasoulis, A., Hall, T. M., Vijayakumar, S., Jackson, A. & Nazarpour, K. Generalizability of EMG decoding using local field potentials. in *2014 36th Annual International Conference of the IEEE Engineering in Medicine and Biology Society* 1630–1633 (IEEE, 2014).

66. Churchland, M. M. *et al.* Neural population dynamics during reaching. *Nature* **487**, 51–56 (2012).

67. Frohlich, J., Toker, D. & Monti, M. M. Consciousness among delta waves: a paradox? *Brain* **144**, 2257–2277 (2021).

68. Kim, J. *et al.* Recovery of consolidation after sleep following stroke—interaction of slow waves, spindles, and GABA. *Cell Rep* **38**, (2022).

69. Shen, G. *et al.* Decoding the individual finger movements from single-trial functional magnetic resonance imaging recordings of human brain activity. *European Journal of Neuroscience* **39**, 2071–2082 (2014).

70. Alazrai, R., Alwanni, H. & Daoud, M. I. EEG-based BCI system for decoding finger movements within the same hand. *Neurosci Lett* **698**, 113–120 (2019).

71. Xiao, R. & Ding, L. Evaluation of EEG features in decoding individual finger movements from one hand. *Comput Math Methods Med* **2013**, 243257 (2013).

72. Stankevich, L. A. *et al.* EEG pattern decoding of rhythmic individual finger imaginary movements of one hand. *Hum Physiol* **42**, 32–42 (2016).

73. Nambu, I. *et al.* Decoding sequential finger movements from preparatory activity in higher-order motor regions: a functional magnetic resonance imaging multi-voxel pattern analysis. *European Journal of Neuroscience* **42**, 2851–2859 (2015).

74. Baillet, S. Magnetoencephalography for brain electrophysiology and imaging. *Nat Neurosci* **20**, 327–339 (2017).

75. Komorowski, R. W., Manns, J. R. & Eichenbaum, H. Robust conjunctive item–place coding by hippocampal neurons parallels learning what happens where. *Journal of Neuroscience* **29**, 9918–9929 (2009).

76. Georgopoulos, A. P. Population activity in the control of movement. *Int Rev Neurobiol* 103 (1994).

77. AP, G. On the relations between the direction of two-dimensional arm movements and cell discharge in primate motor cortex. *J Neurosci* **2**, 1527–1537 (1982).

78. Pan, S. C. & Rickard, T. C. Sleep and motor learning: Is there room for consolidation? *Psychol Bull* **141**, 812 (2015).

79. Jacobacci, F. *et al.* Rapid hippocampal plasticity supports motor sequence learning. *Proceedings of the National Academy of Sciences* **117**, 23898–23903 (2020).

80. Brooks, E., Wallis, S., Hendrikse, J. & Coxon, J. Micro-consolidation occurs when learning an implicit motor sequence, but is not influenced by HIIT exercise. *NPJ Sci Learn* **9**, 23 (2024).

81. Robertson, E. M. Skill memory: mind the ever-decreasing gap for offline processing. *Current Biology* **29**, R287–R289 (2019).

82. Chen, P.-C., Stritzelberger, J., Walther, K., Hamer, H. & Staresina, B. Hippocampal ripples during offline periods predict human motor sequence learning. *bioRxiv* 2010–2024 (2024).

83. Johnson, B. P. *et al.* Generalization of procedural motor sequence learning after a single practice trial. *NPJ Sci Learn* **8**, 45 (2023).

84. Rickard, T. C., Cai, D. J., Rieth, C. A., Jones, J. & Ard, M. C. Sleep does not enhance motor sequence learning. *J Exp Psychol Learn Mem Cogn* **34**, 834 (2008).

85. Das, A., Karagiorgis, A., Diedrichsen, J., Stenner, M.-P. & Azanon, E. “Micro-offline gains” convey no benefit for motor skill learning. *bioRxiv* 2024–2027 (2024).

86. Gupta, M. W. & Rickard, T. C. Comparison of online, offline, and hybrid hypotheses of motor sequence learning using a quantitative model that incorporate reactive inhibition. *Sci Rep* **14**, 4661 (2024).

87. Gupta, M. W. & Rickard, T. C. Dissipation of reactive inhibition is sufficient to explain post-rest improvements in motor sequence learning. *NPJ Sci Learn* **7**, 25 (2022).

88. Ruiz, M. H., Jabusch, H.-C. & Altenmüller, E. Detecting wrong notes in advance: neuronal correlates of error monitoring in pianists. *Cerebral cortex* **19**, 2625–2639 (2009).

89. Maidhof, C., Rieger, M., Prinz, W. & Koelsch, S. Nobody is perfect: ERP effects prior to performance errors in musicians indicate fast monitoring processes. *PLoS One* **4**, e5032 (2009).

90. Censor, N., Horovitz, S. G. & Cohen, L. G. Interference with existing memories alters offline intrinsic functional brain connectivity. *Neuron* **81**, 69–76 (2014).

91. Oostenveld, R., Fries, P., Maris, E. & Schoffelen, J.-M. FieldTrip: open source software for advanced analysis of MEG, EEG, and invasive electrophysiological data. *Comput Intell Neurosci* **2011**, 1–9 (2011).

92. Delorme, A. & Makeig, S. EEGLAB: an open source toolbox for analysis of single-trial EEG dynamics including independent component analysis. *J Neurosci Methods* **134**, 9–21 (2004).

93. Rijsbergen, V. Information retrieval; ; Butterworth, 1978. *J. librariansh.* **11**, 237 (1979).

94. Schütze, H., Manning, C. D. & Raghavan, P. Introduction to information retrieval cambridge university press cambridge. (2008).

95. Ding, C. & Peng, H. Minimum redundancy feature selection from microarray gene expression data. *J Bioinform Comput Biol* **3**, 185–205 (2005).

96. Holland, P. W. & Welsch, R. E. Robust regression using iteratively reweighted least-squares. *Communications in Statistics-theory and Methods* **6**, 813–827 (1977).

97. Iwane, F., Buch, R., Cohen, L. Sequence regularity determines if early learning gains occur during practice or rest. Program No. PSTR369.21. 2024 Neuroscience Meeting Planner. Chicago, IL. : Society for Neuroscience, 2024. Online.

Supplementary Materials

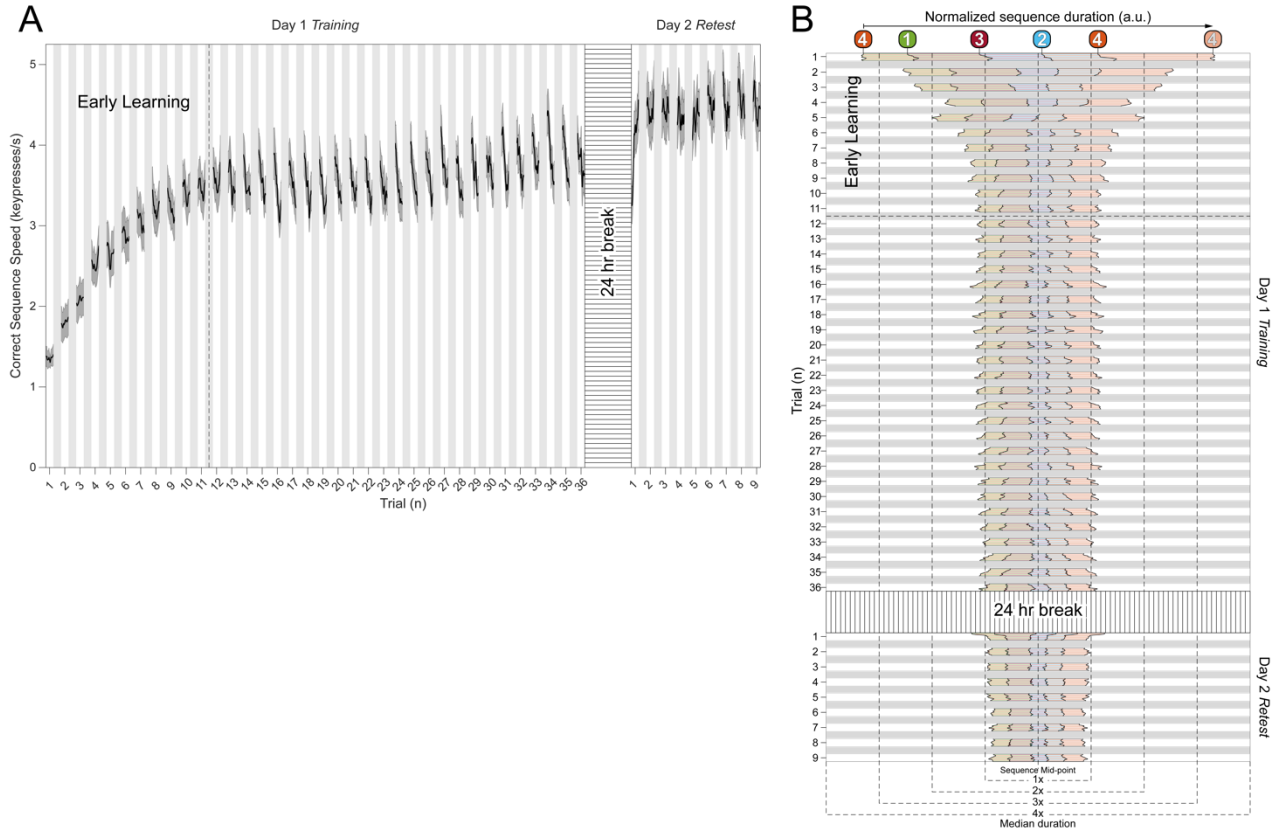

Figure 1 – figure supplement 1: Behavioral performance during skill learning. ***A. Total Skill Learning over Day 1 Training (36 trials) and Day 2 Retest (9 trials)***. As reported previously[1], participants on average reached 95% of peak performance during *Day 1 Training* by trial 11. Note that after trial 11 performance stabilizes around a plateau through trial 36. Following a 24-hour break, participants displayed an upward shift in performance during the *Day 2 Retest* – indicative of an overnight skill consolidation effect. ***B. Keypress transition time (KTT) variability.*** Distribution of KTTs normalized to the median correct sequence time for each participant and centered on the mid-point for each full sequence iteration during early learning. Note that the initial variability of the five component transitions in the sequence (i.e. – 4-1, 1-3, 3-2, 2-4, 4-4) stabilize by trial 6 in the early learning period and remain stable throughout the rest of *Day 1 Training* (through trial 36) and *Day 2 Retest*.

Intra-parcel Decoder
High Gamma (51-100 Hz)
Gamma (25-50 Hz)
Beta (15-24 Hz)
Alpha (8-14 Hz)
Theta (4-7 Hz)
Delta (1-3 Hz)
Broadband (1-100 Hz)
Left Hemisphere
Right Hemisphere
Transverse temporal sulcus
Superior temporal sulcus
Inferior temporal sulcus
Subparietal sulcus
Suborbital sulcus
Superior part of the precentral sulcus
Inferior part of the precentral sulcus
Postcentral sulcus
Pericallosal sulcus
Parieto-occipital sulcus
Orbital sulci
Medial orbital sulcus
Lateral orbital sulcus
Medial occipito-temporal sulcus and lingual sulcus
Lateral occipito-temporal sulcus
Anterior occipital sulcus and preoccipital notch
Superior occipital sulcus and transverse occipital sulcus
Middle occipital sulcus and lunatus sulcus
Intraparietal sulcus and transverse parietal sulci
Sulcus intermedius primus
Superior frontal sulcus
Middle frontal sulcus
Inferior frontal sulcus
Posterior transverse collateral sulcus
Anterior transverse collateral sulcus
Superior segment of the circular sulcus of the insula
Inferior segment of the circular sulcus of the insula
Anterior segment of the circular sulcus of the insula
Marginal branch of the cingulate sulcus
Central sulcus
Calcarine sulcus
Temporal pole
Occipital pole
Posterior ramus of the lateral sulcus
Vertical ramus of the anterior segment of the lateral sulcus
Horizontal ramus of the anterior segment of the lateral sulcus
Middle temporal gyrus (T2)
Inferior temporal gyrus (T3)
Planum temporale of the superior temporal gyrus
Planum polare of the superior temporal gyrus
Lateral aspect of the superior temporal gyrus
Anterior transverse temporal gyrus
Subcallosal area of the subcallosal gyrus
Straight gyrus
Precuneus
Precentral gyrus
Postcentral gyrus
Superior parietal lobule
Supramarginal gyrus
Angular gyrus
Orbital gyri
Parahippocampal gyrus (T5)
Lingual gyrus (O5)
Fusiform gyrus (O4-T4)
Superior occipital gyrus (O1)
Middle and lateral occipital gyrus (O2)
Short insular gyri
Long insular gyrus and central sulcus of the insula
Superior frontal gyrus (F1)
Middle frontal gyrus (F2)
Triangular part of the inferior frontal gyrus
Orbital part of the inferior frontal gyrus
Opercular part of the inferior frontal gyrus
Cuneus (O6)
Ventral part of the posterior cingulate gyrus (vPCC)
Dorsal part of the posterior cingulate gyrus (dPCC)
Posterior part of the middle cingulate gyrus and sulcus (pMCC)
Anterior part of the middle cingulate gyrus and sulcus (aMCC)
Anterior cingulate gyrus and sulcus (ACC)
Transverse frontopolar gyri and sulci
Subcentral gyrus and sulci
Paracentral lobule and sulcus
Inferior occipital gyrus (O3) and sulcus
Fronto-marginal gyrus and sulcus
35
40
45
50
55
60
65
Decoding Accuracy (%)

1079

Figure 2 – figure supplement 1: Oscillatory contributions at individual brain regions. Decoding performance of each individual brain region (intra-parcel decoder performance) at each oscillatory level is shown for both left and right hemisphere as a heatmap. Optimal decoding performances were obtained from bilateral superior frontal (Left: 68.77% ± SD 7.6%; Right: 67.52% % ± SD 6.78%), middle frontal (Left: 63.41% ± SD 7.58%; Right: 62.78% % ± SD 76.94%), pre-central (Left: 62.37% % ± SD 6.32%; Right: 62.69% ± SD 5.94%), and post-central (Left: 61.71% ± SD 6.62%; Right: 61.09% ± SD 6.2%) brain regions. Superior parietal, central, paracentral, anterior-cingulate, and precuneus regions also showed greater (> 60%) decoding performance. For Delta band, only superior frontal regions showed > 60% decoding performance.

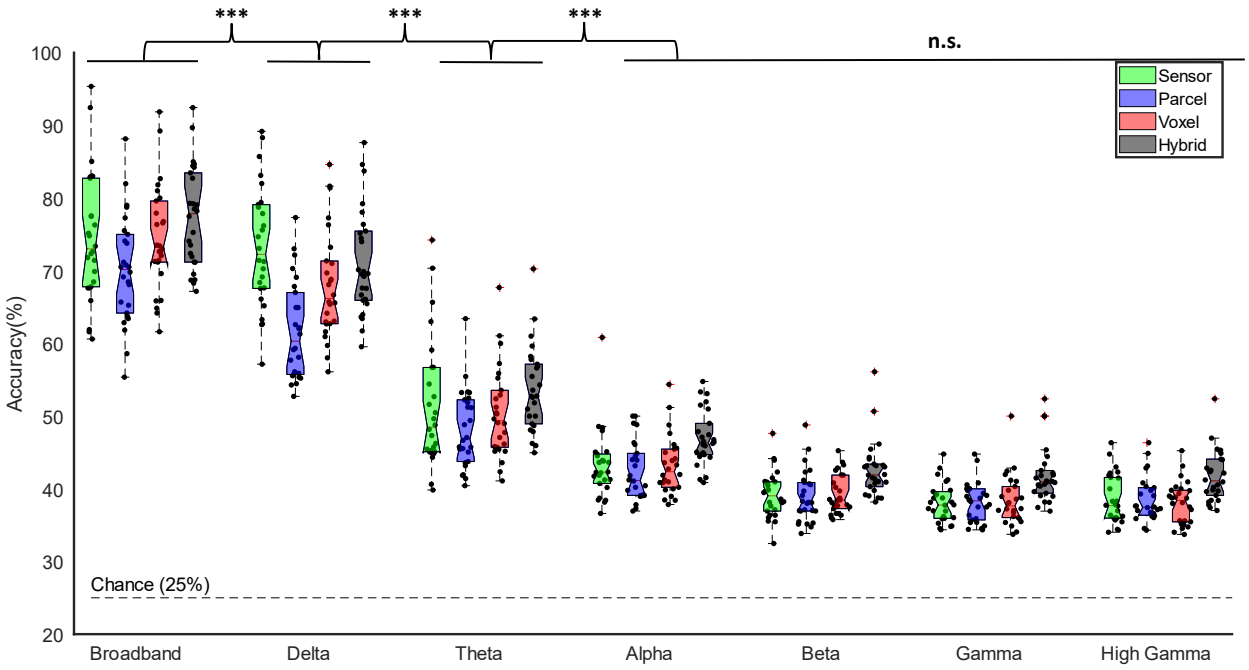

Figure 3—figure supplement 1: Contribution of whole-brain oscillatory frequencies to decoding. Accuracy was highest when decoders were trained on broadband activity, closely followed by delta band activity, across whole-brain -parcel, -voxel, and -hybrid space. Sensor-space decoder accuracy did not differ statistically when trained on either broadband or delta-band activity. Hybrid approach resulted in best decoding accuracy for each frequency range. Interestingly, accuracy with sensor space decoders was comparable to accuracy with parcel and voxel space decoders. Dots depict decoding accuracy for each participant. "***" indicates $p < 0.001$, "**" indicates $p < 0.01$, and "**n.s.**" denotes no statistical significance (i.e. - $p > 0.05$).

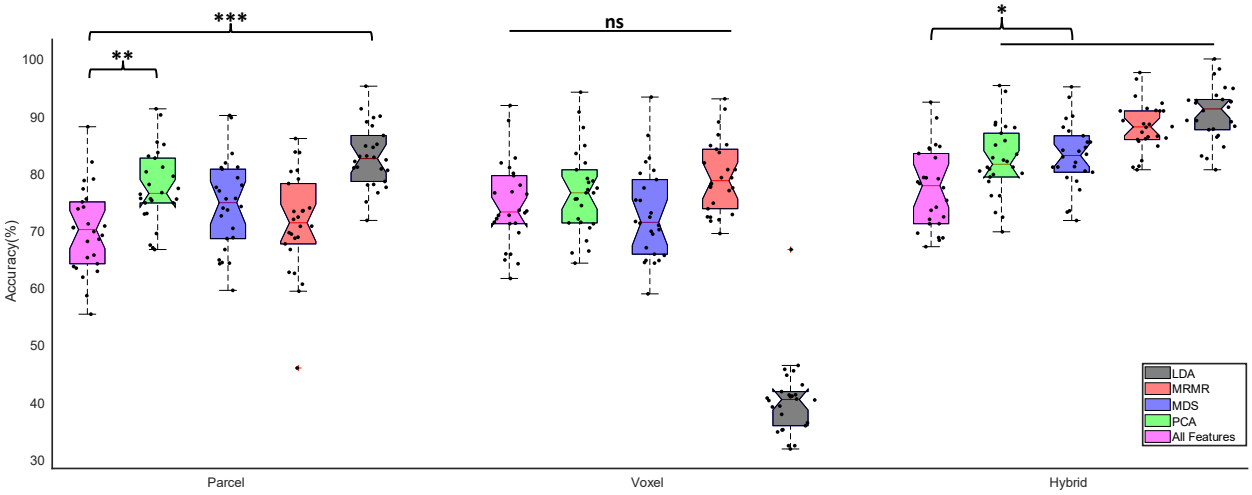

Figure 3 – figure supplement 2: Comparison of different dimensionality reduction techniques. Dimensionality reduction was applied to the input features for each approach [parcel (N=148)/voxel(N=15684)/hybrid(N=1295)] [1]. The results with principal component analysis (PCA, in green), multi-dimensional scaling (MDS, in blue), minimum redundant maximum relevance algorithm (MRMR, in red), linear discriminant analysis (LDA, in black) are shown in comparison to performance obtained using all input features (in magenta). For parcel space, all these approaches increased the mean decoding accuracy with PCA and LDA showing statistically significant improvement [1-way ANOVA: F= 13.05, $p < 0.001$; post hoc Tukey tests: p =0.032 (PCA), $p < 0.001$ (LDA), $p > 0.05$ (MDS, MRMR)]. At the voxel space, there was no statistically significant improvement with either of the approaches ($p > 0.05$). MRMR showed the highest improvement but not statistically significant with post hoc Tukey tests ($p = 0.14$). With LDA the performance dropped significantly. For hybrid space, all the dimensionality reduction techniques were significant in improving decoding performance [1-way ANOVA: F= 21.32, post hoc Tukey tests: $p < 0.05$] and the best improvement was seen with LDA.

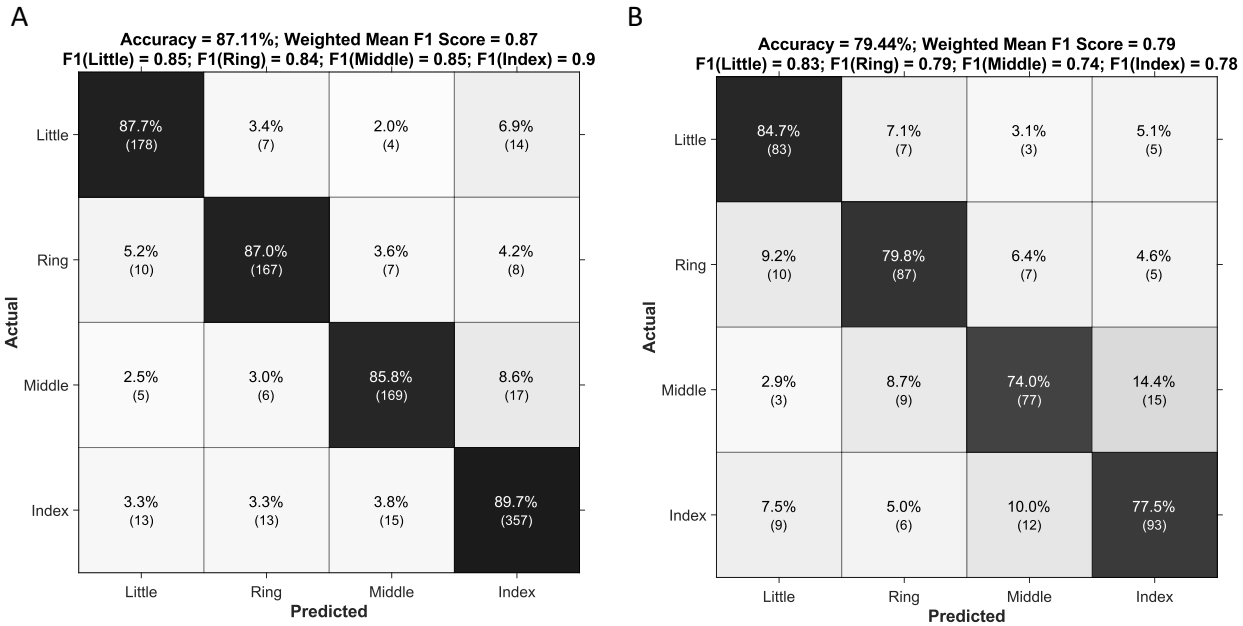

Figure 3 – figure supplement 3: Confusion matrices for decoding performance on Day 2 Retest (A) and Day 2 Control (B) data. Note that, the hybrid decoding strategy generalized to Day 2 data with 87.11% keypress decoding accuracy for the trained sequence (Day 2 Retest) and 79.44% accuracy for decoding keypresses embedded within untrained control sequences (Day 2 Control).

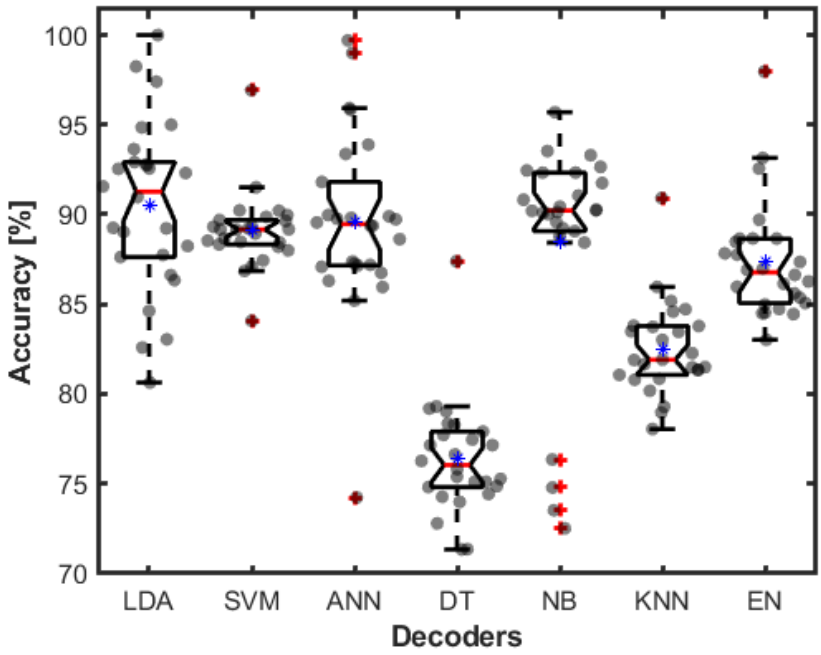

Figure 3 – figure supplement 4: Comparison of different decoder methods. Performance for different decoders used is shown for each participant. The results show that linear discriminant analysis classifier (LDA) was the optimal choice. Results from LDA decoder analyses were used for all subjects and results reported in the manuscript.

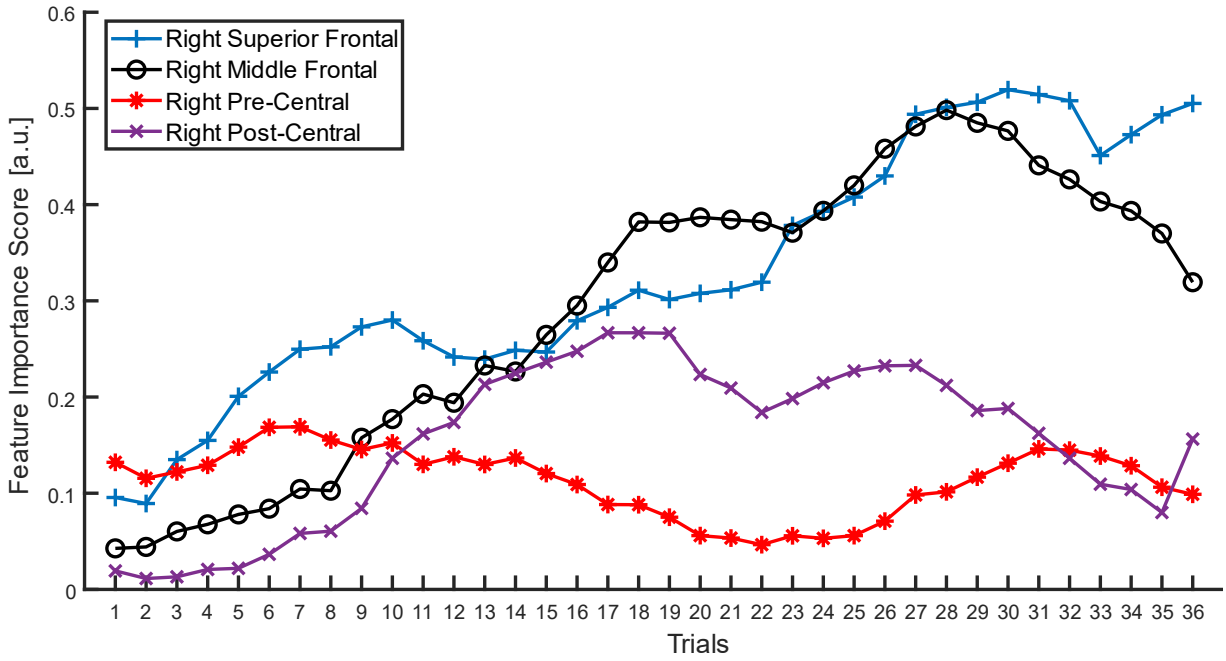

Figure 4 – figure supplement 1: Quantification of regional trial-by-trial feature importance score during skill learning. The quantification of regional importance in decoding for each trial is shown for the regions that showed highest decoding accuracy, i.e., superior frontal, middle frontal, pre-central, and post-central cortex. Please note that, the feature importance score was higher for pre-central cortex which shifted to middle frontal cortex during later trials, as can be seen with the divergence of line plots about trial 11.

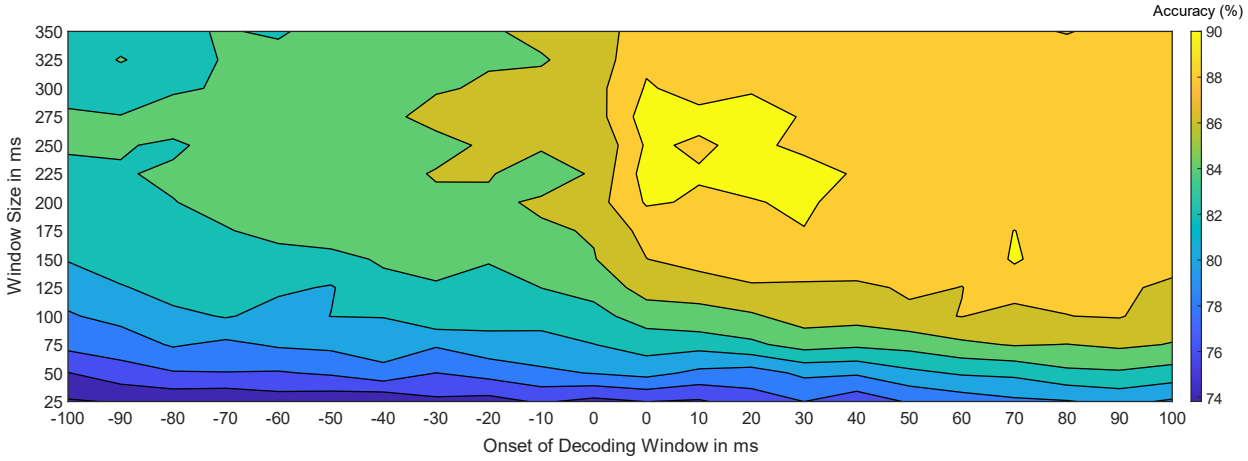

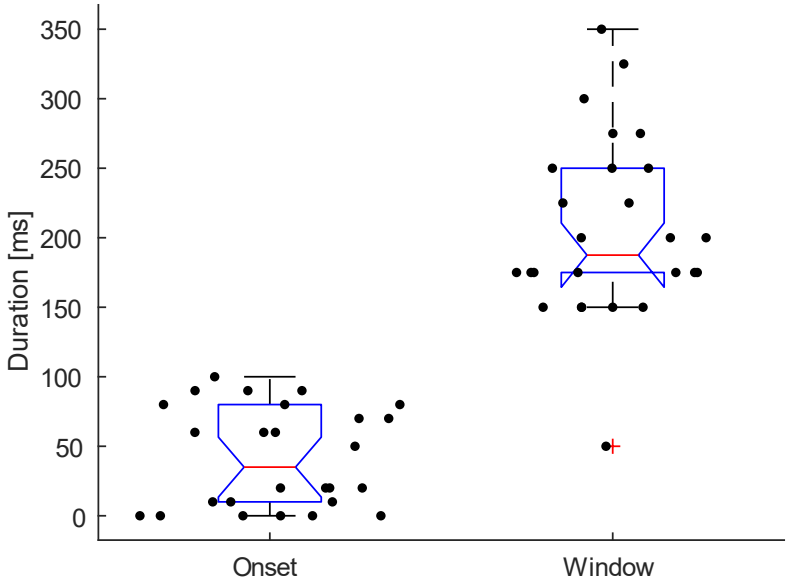

Figure 4 – figure supplement 2: Average decoding accuracies across participants with varying window parameters (top panel). X-axis represents the onset of window for decoding analysis with respect to keypress onset (0). Y-axis represents the window size. The heatmap color denotes the decoding accuracy for all window size/location pairings. Note that, the best decoding accuracy across subjects is obtained by taking a window starting from 0 (i.e., onset of keypress) with a window size of 200ms. The windowing parameters used for each subject in reported results are shown in the bottom panel.

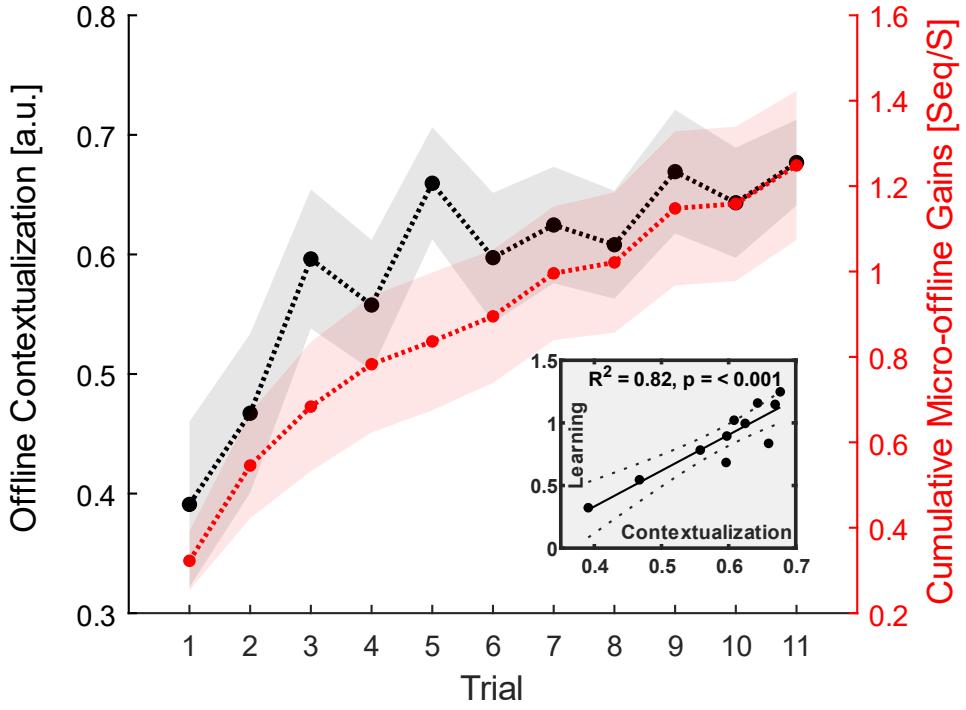

Figure 5. figure supplement 1. Relationship between offline neuronal representational change and micro-offline learning. Cumulative micro-offline gains, i.e., the net gain in skill during inter-practice rest periods increased over time during early learning. Offline representation difference, i.e., the net change in the neural representations of keypress 4 over the inter-practice rest intervals between different ordinal positions in the sequence (context) increased over time during early learning. A linear regression analysis showed a strong temporal relationship (correlation coefficient (r) = 0.9034 and coefficient of variance explained (R^2) = 0.82) between amount of contextualization during rest and cumulative micro-offline gains during rest, signifying the effect of contextualization in sequential skill learning.

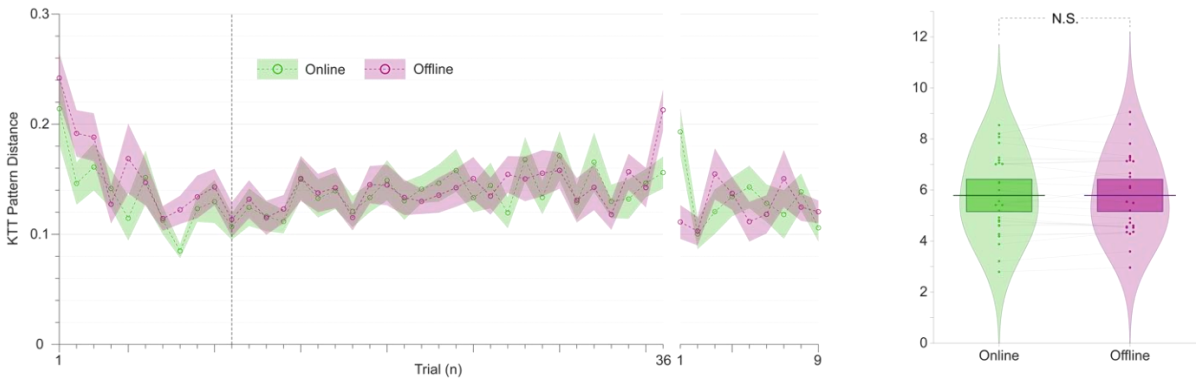

Figure 5 – figure supplement 2: Online versus offline changes in keypress transition patterns. A. Trial-by-trial Euclidian distance between keypress transition patterns (i.e. – relative share of each keypress transition across the full sequence duration) for the first and last sequence iteration within a single trial (online; green) and last sequence iteration of the current trial versus the first sequence iteration of the subsequent trial (offline; magenta). B. Cumulative online (green; left) and offline (magenta; right) pattern distances recorded over all forty-five trials covering Days 1 and 2. Note that cumulative online and offline distances are not significantly different (t=-0.03, p = 0.976).

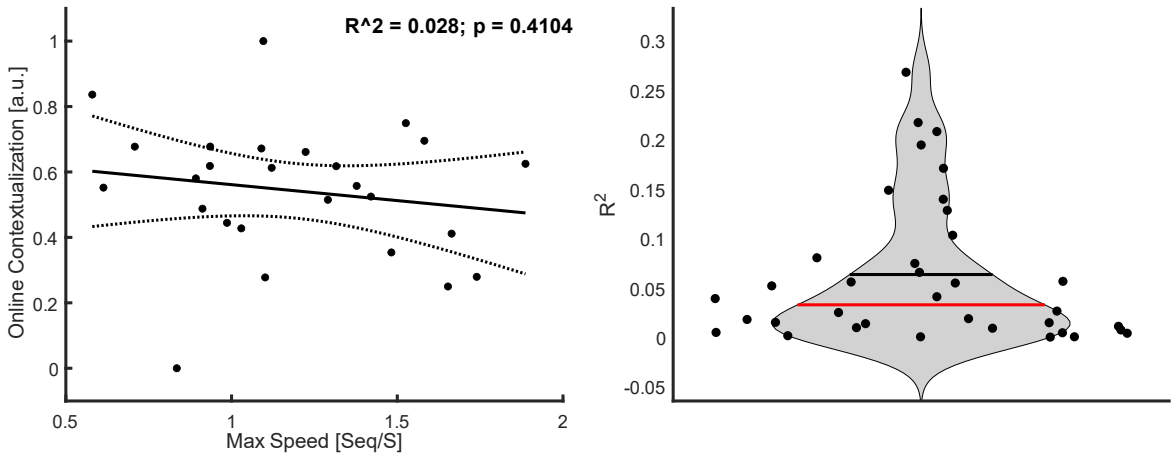

Figure 5 – figure supplement 3: Relationship between contextualization and absolute speed. ***A. Relationship between maximum speed and corresponding contextualization:*** The maximum typing speed and the degree of contextualization was related using a linear regression analysis that showed no significant relationship between maximum typing speed and degree of contextualization ($R^2 = 0.028$, $p = 0.41$). Here, each dot represents the maximum speed attained and the corresponding degree of contextualization of each participant. Thus, people with higher typing speed did not show higher degree of contextualization. ***B. Relationship between typing speed and degree of contextualization at each trial.*** We performed a regression analysis for each trial to relate the degree of contextualization at each trial and the typing speed at that trial. The violin plot represents the distribution of R^2 values obtained with regression analysis and here each dot represents a trial. Note that, there was no significant relationship at any trial (mean $R^2 = 0.06$; $p > 0.05$).

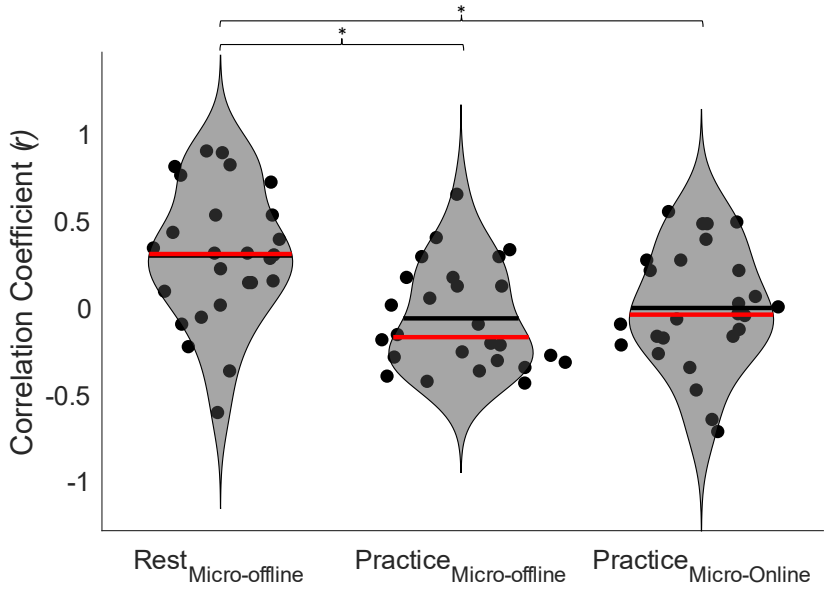

Figure 5 – figure supplement 4: Distribution of individual subject correlation coefficients between contextualization changes occurring during practice or rest with micro-online and micro-offline performance gains. The correlation distributions were significantly higher for the relationship between contextualization changes during rest and micro-offline gains than for contextualization changes during practice with either micro-online or micro-offline gains.

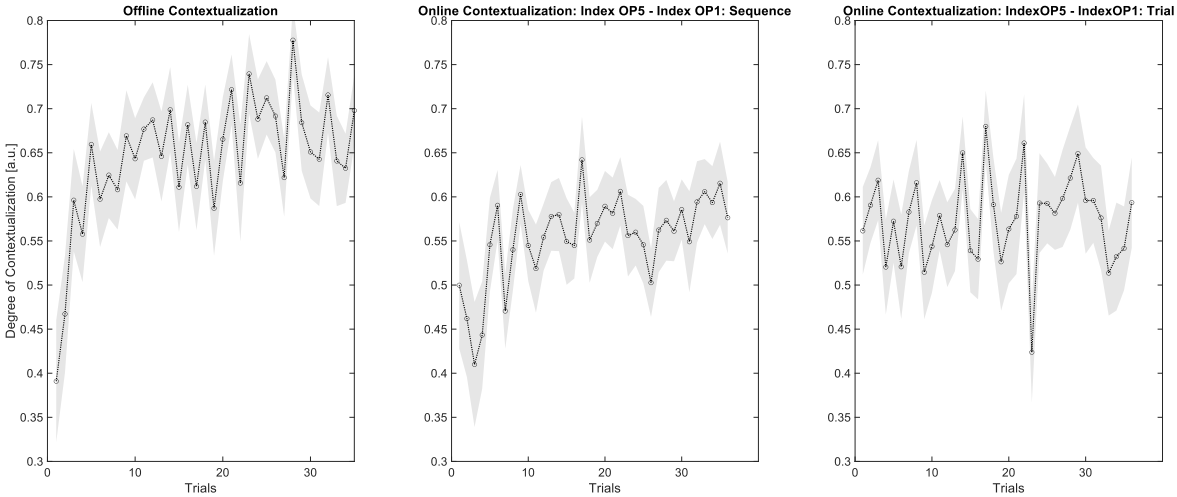

Figure 5 – figure supplement 5: Trial by trial trend of offline (left panel) and online (middle and right panels) contextualization changes. Offline contextualization changes were assessed by calculating the distance between neural representations for the last $\text{Index}_{\text{OP5}}$ keypress in the previous trial and the first $\text{Index}_{\text{OP1}}$ keypress in the present trial. Two different approaches were used to characterize online contextualization changes. The analysis included in the reviewed manuscript (middle panel) calculated the distance between $\text{Index}_{\text{OP1}}$ and $\text{Index}_{\text{OP5}}$ for each correct sequence, which was then averaged across the trial. This approach is limited by the lack of control for the passage of time when making online versus offline comparisons. Thus, the second approach controlled for the passage of time by calculating distance between the representations associated with the first $\text{Index}_{\text{OP1}}$ keypress and the last $\text{Index}_{\text{OP5}}$ keypress within the same trial. Note that while the first approach showed an increase online contextualization trend with practice, the second approach did not.

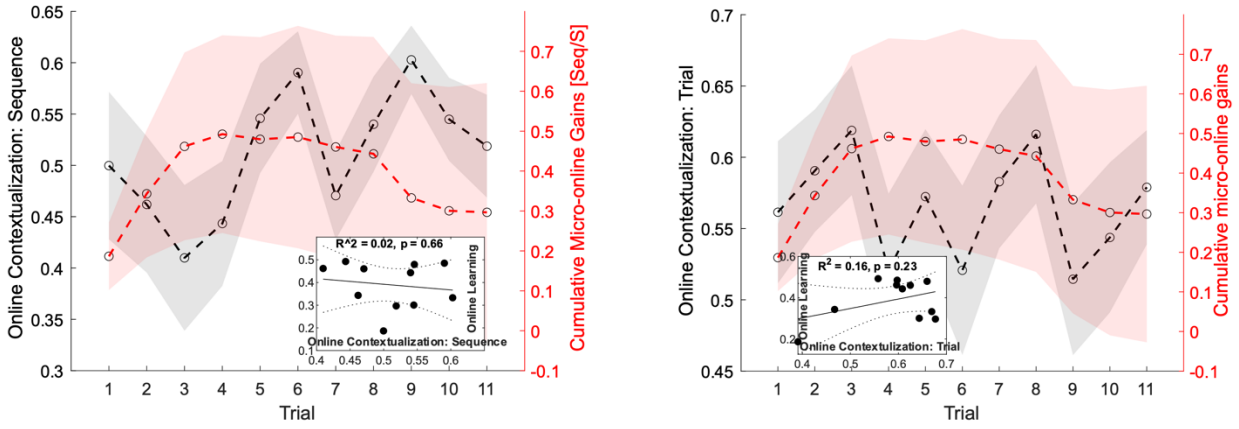

Figure 5 – figure supplement 6: Online contextualization versus micro-online learning. The relationship between online contextualization and online learning is shown for both within-sequence (left) and across-sequence (right) distance calculation. There was no significant relationship between online learning and online contextualization regardless of the measurement approach.